Journal of Applied Geophysics 167 (2019) 73–105

Contents lists available at ScienceDirect

Journal of Applied Geophysics

journal homepage: www.elsevier.com/locate/jappgeo

New insights on subsurface geological and tectonic structure of the Athens basin (Greece), derived from urban gravity measurements

Spyridon Dilalos [a,*], John D. Alexopoulos [a], Stylianos Lozios [b]

[a] National and Kapodistrian University of Athens, Department of Geology and Geoenvironment, Division of Geophysics-Geothermic, Panepistiomioupoli Zografou, Greece
[b] National and Kapodistrian University of Athens, Department of Geology and Geoenvironment, Division of Dynamic Tectonic & Applied Geology, Panepistiomioupoli Zografou, Greece

ARTICLE INFO

Article history:
Received 7 December 2018
Received in revised form 6 March 2019
Accepted 30 April 2019
Available online 16 May 2019

Keywords:
Gravity method
Density determination
Nettleton profiles
Structural maps
Urban areas
2.75D profile modelling

ABSTRACT

The gravity method has been applied, with a total of 1.122 gravity measurements for the subsurface investigation of the geotectonic structure beneath the urban and sub-urban areas of Athens basin. The aim was to either verify previously mapped concealed fault zones or even discover new concealed faults that may affect the city in the future by generating disastrous earthquakes. Three different methods have been used to determine the densities of the existing geological formations in the best possible way: laboratory measurements, Nettleton profiles and the seismic velocity conversion. In the context of the qualitative interpretation, we took advantage of the derivatives methods in order to enhance the structural edges of density sources that may reflect fault zones. Thereby, several structural maps have been produced by applying most of the enhancement techniques, such as the Total Horizontal Derivative (*THDR*), the First Vertical Derivative (*VDR*), the Second Vertical Derivative (*SVDR*), the Analytical Signal (*AS*), Tilt (*Tilt*) and the Theta (cos *Tilt*). Their results were extremely helpful, providing severe indications for the delineation of the fault pattern of the area. These results were combined with interpretive geological 2.75-D density models in order to verify or modify fault regime of the area. Important data regarding the geological and tectonic structure beneath the Quaternary formations were retrieved. More specifically, we were able to verify and modify the locations and lengths of already proposed as concealed faults zones from older geological researches or even better to identify and propose new locations of concealed faults that have not been identified so far.

1. Introduction

The present gravity study was conducted in the Athens basin (Greece), with the aim of investigating its geological and tectonic structure and identifying potential faults (blind or covered), which could affect the city in the future by causing disastrous earthquakes. On 7th September 1999, a 5.9 Richter earthquake occurred in the Greek metropolis of Athens, causing extensive damage to almost 70.000 buildings, with almost 100 of them collapsing (Bouckovalas and Kouretzis, 2001). More than 2.000 people were injured along with 143 fatalities and at least 100.000 people left homeless. Following the event, a number of geological researches began in the area, but the Athens basin is extensively urbanized. Applying geophysical methods such as electromagnetics, magnetics and geoelectrics can be challenging in this urban environment. On the other hand, the gravity method has been widely applied within the last few years contributing to the investigation of basin structure with some of them localized beneath urbanized areas (Anderson et al., 2004; de Castro et al., 2014; Hosseini et al., 2013; Khamies and El-Tarras, 2010; Koumetio et al., 2012; McPhee et al., 2007; Nasr et al., 2011; Park et al., 2006). For these reasons, through the acquisition of gravity measurements, covering for the first time all the area of Athens basin, the authors tried to collect as much information as possible regarding the geotectonic regime of Athens basin subsurface.

The application of geophysical methods in the area of Athens basin, based on the existing literature has mostly focused on engineering and archaeological applications (Apostolopoulos et al., 2014; Louis et al., 2002a, 2002b; Papadopoulos et al., 2001; Papaioannou, 2002; Symeonidis et al., 2005; Tsokas et al., 2008; Tsourlos and Tsokas, 2011). A local but relatively deeper investigation has been carried out with the application of geoelectrical method by Alexopoulos et al. (2001) who adumbrated a couple of possible blind faults in the area of Tatoi. Finally, Papadopoulos (2003), Papadopoulos et al. (2007) acquired a few profiles of seismic and gravity measurements along the basins of Thriassio and Athens. Their preliminary results revealed the large thickness (almost 800 m) of post-alpine sediments NE of *Thrakomakedones* while their qualitative interpretation of gravity anomalies indicated the existence of some possible fault zones in the greater areas of *Kamatero* and *Acharnes*.

* Corresponding author.
E-mail addresses: sdilalos@geol.uoa.gr (S. Dilalos), jalexopoulos@geol.uoa.gr (J.D. Alexopoulos), slozios@geol.uoa.gr (S. Lozios).

https://doi.org/10.1016/j.jappgeo.2019.04.024
0926-9851/

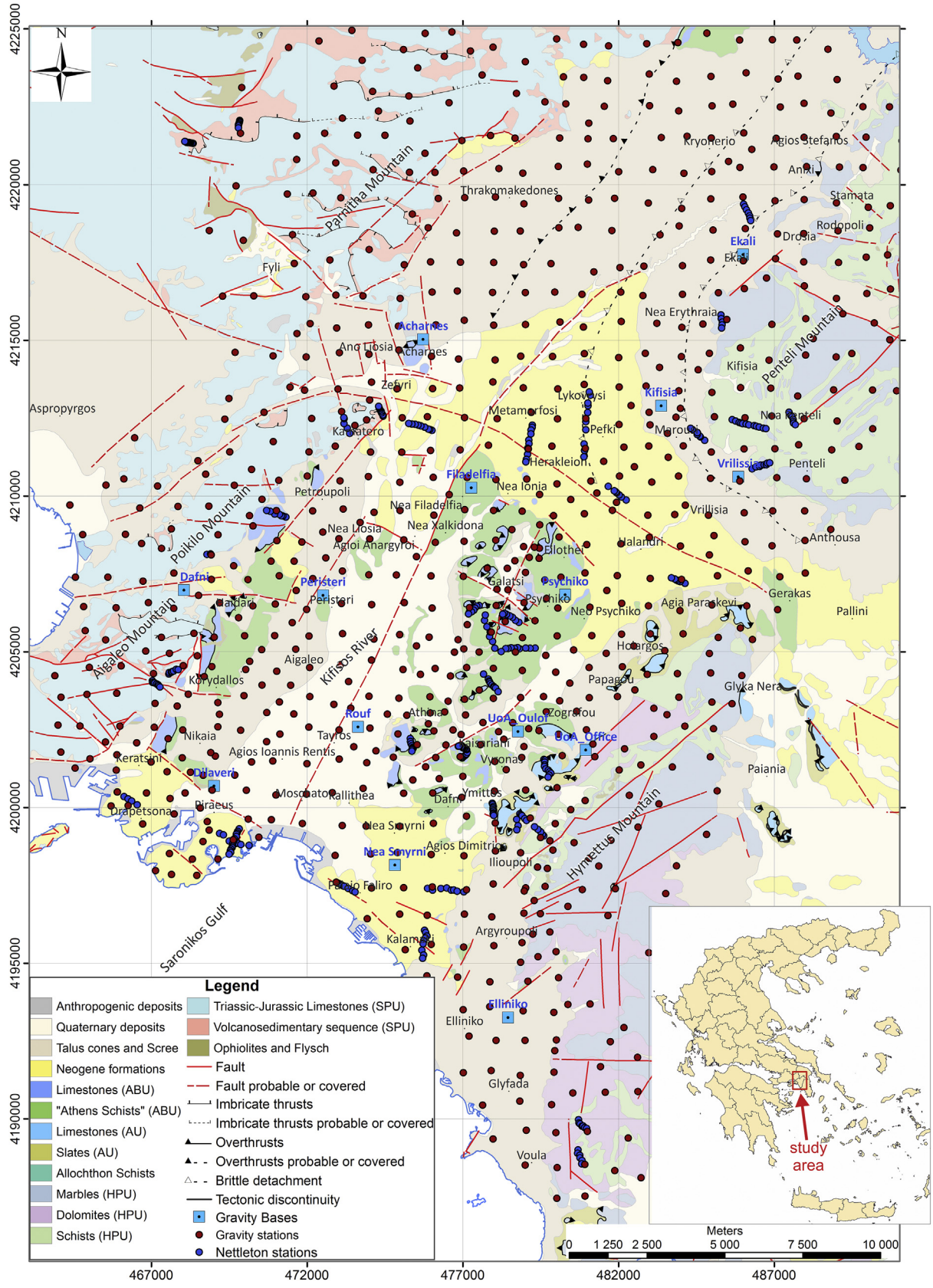

Fig. 1. Modified geological and tectonic map (Dilalos, 2018), with the locations of gravity measurements. An index map of Greece and the location of the study areas are also provided.

2. Geological and tectonic setting

The Athens basin hosts the metropolis of Greece, with a population of up to 4 million people in an area of almost 360 km^2, surrounded by the mountains Aigaleo and Poikilo (*West*), Parnitha (*North*), Penteli (*Northeastern*) and Hymettus (*East*). Despite the great number of papers published on the geological structure of Athens (Freyberg, 1951; Lekkas and Lozios, 2000; Lepsius, 1893; Lozios, 1993; Mariolakos and Fountoulis, 2000; Marinos et al., 1971, 1974; Niedermayer, 1971; Sabatakakis, 1991), questions still remain unanswered, especially in light of the 1999 earthquake. After the earthquake, a new updated and more detailed geologic and neotectonic mapping was assigned to Papanikolaou et al., 2002 This map was modified and simplified by Dilalos (2018) in the context of this gravity survey, but also completed and combined with some of the existent studies where there was no coverage (Fig. 1).

The geological and geotectonic structure is quite complicated since at least four alpine geotectonic units (metamorphosed or not) and a thick Neogene sequence form the Athens basin and the surrounding mountainous region. The lower and relative autochthonous "*Hymettus-Penteli Unit*" (*HPU*), occupies the eastern margin of Athens basin (Hymettus and Penteli mountains), and consists mostly of marbles, dolomites, schists, quartzo-feldspathic and metabasic rocks, metamorphosed under a blueschist HP/LT metamorphic event followed by a greenschist-facies overprint, during the Late Cretaceous-Tertiary alpine orogenic event. Parts of this unit seem to be correlative either with the Cycladic Blueschist Unit (*CBU*) or with the Basal Unit of the Attic-Cycladic metamorphic core complex (Altherr et al., 1982; Dürr et al., 1978; Kessel, 1990; Lozios, 1993; Papanikolaou et al., 2002, 2004b). Kilometer-scale isoclinal recumbent folds, concluding in successive, hundreds of meters, alternations between the marbles and the schists, determine the main fold pattern (Lekkas and Lozios, 2000; Lozios, 1993). The overlying unmetamorphosed rocks of "*Sub-Pelagonian Unit*" (*SPU*) are located along the western part of Athens basin (Aigaleo, Poikilo and Parnitha mountains) including Triassic-Jurassic limestones and an Upper Paleozoic-Lower Triassic volcanosedimentary sequence of sandstones, conglomerates, keratophyre tuffs, lavas and olistoliths of limestones. Three or more successive imbricate thrusts, between the limestones and the volcanosedimentary sequence, characterize the tectonic structure of the whole area (Papanikolaou, 2015; Papanikolaou et al., 2002, 2004b). Along the western flanks of Hymettus Mt. and above the relative autochthonous Hymettus-Penteli Unit, the "*Alepovouni Unit*" (*AU*) exists, consisting of very-low grade metamorphic rocks, such as marbles, slates and phyllites. Smaller scattered outcrops of Alepovouni Unit, at the eastern part of Athens basin, also occurred. Finally, the so-called "*Athens Basin Unit*" (*ABU*) represents the upper tectonic unit because it occurs in the form of small-scale outcrops within the Neogene formations of Athens basin. It includes various lithological types, such as limestones, marbles, sandstones, slates (called as "*Athens Schists*"), serpentinites and basic rocks, in the form of a tectonic mélange, which tectonically overlie both the SPU, along the western margin of Athens Basin and the *HPU*, along the eastern part of Athens basin (Lekkas and Lozios, 2000; Papanikolaou, 2015; Papanikolaou et al., 2002, 2004b).

The exhumation of Hymettus-Penteli metamorphics is controlled by a crustal-scale detachment fault, which is considered to be part of the Western Cycladic Detachment System (*WCDS*), (Coleman et al., 2018; Grasemann et al., 2012; Iglseder et al., 2011; Lekkas et al., 2011; Seman et al., 2012, 2013). The "*Alepovouni*", "*Athens Basin*" and "*Sub-Pelagonian*" are lightly to unmetamorphosed geotectonic units and reside in the hanging wall of the detachment fault (resulting in more complicated structure and heterogeneity) and the "*Hymettus-Penteli*" is medium to high grade metamorphosed unit to the footwall (lower plate). The detachment zone has a thickness of a few meters (max 40 m) and, in some cases, it is branched into two or more strands. It is easily recognizable to the field, in a lot of places all around Hymettus Mt., by the mylonitic or ultramylonitic character of Hymettus-Penteli unit rocks (marbles, dolomites or schists) and characteristic brittle-ductile shear structures. The contacts between the geotectonic units of the upper plate have an initial contractional character (thrust faults) during the formation of the alpine nappe pile and a latter extensional stage where they reactivated as brittle low-angle normal faults, during the exhumation of Hymettus-Penteli metamorphic core (Coleman et al., 2018; Krohe et al., 2010; Lekkas et al., 2011; Papanikolaou et al., 2002).

The post-alpine Neogene and Quaternary formations occupy the major area of the basin, with the exception of some remaining hills in the central part (*Filopappou*, *Acropolis*, *Lycabettus*, *Ardittou*, *Tourkovounia*, *Kokkou*), constituted mainly by the "*Athens Basin Unit*". Papanikolaou et al. (2002) had proposed more than ten different post-alpine formations but here they are simplified by similar density (Dilalos, 2018). Their thickness varies from a few meters to several hundred of meters and conglomerates, marls, sandstones and marly limestones represent the most common lithologies.

The Quaternary deposits (alluvial deposits, scree, talus cones, fluviatile deposits and terraces) occupy a large part of the basin, covering a number of alpine and neotectonic faults and fault zones. For example, the wide zone where the *Kifisos* River flows conceals the expected location of the detachment fault between the *HPU* metamorphics and the overlying *SPU*, beneath the Quaternary deposits and Neogene formations. This major and important tectonic structure has been mapped only to the North of our research area (NE Attica and Southern Evia) but it is expected to continue southern, through the Athens basin, covered by the post-alpine deposits and possibly the two slightly metamorphosed units ("*Alepovouni*" and "*Athens Basin*"). Additionally, during earlier geophysical investigations and drilling projects in distinct areas, a significant number of neotectonic faults and fault zones have been determined, buried mostly beneath alluvial deposits and talus cones (Alexopoulos et al., 2001; Lekkas et al., 2001; Louis et al., 2002b; Papadopoulos, 2003; Papadopoulos et al., 2007). It is also remarkable that some of these faults appeared to influence the damage distribution during the September 7th, 1999 5,9R earthquake (Lekkas et al., 2001).

The neotectonic pattern includes mainly steep normal faults, which are divided by orientation into two groups. The older group of faults has an NNE-SSW orientation, which coincides with the principal axis of the Athens basin and the main low-angle normal faults between the alpine geotectonic units. The youngest and most active group of faults has strikes that vary from WNW-ESE to NW-SE, in the western and eastern part of the basin, indicating the gradual transition from the major active E-W faults of Eastern Korinthiakos Gulf to the moderate (also active) faults of Southern Evoikos Gulf (Antoniou, 2000; Mariolakos et al., 2001; Papanikolaou and Lozios, 1990; Papanikolaou et al., 2004a).

3. Density determination

Density is the physical quantity that controls the gravity response of each geological formation, based on its characteristics (e.g. porosity, age and metamorphism). Density contrasts of geological formations are very important for the processing of the gravity data and the construction of the gravity models.

3.1. Methods for density determination

In the context of this paper, the density of the existing geological formations in the Athens basin was determined using three different methods, where possible. The laboratory measurements on surface outcrop samples or borehole cores and the Nettleton method were applied to almost every type of geological formation of the Athens basin. Additionally, we managed to estimate the density of some geological formations from conversion of published seismic velocity data.

Several authors (Abzalov, 2013; Baptiste et al., 2016; Boszczuk et al., 2011; Damaceno et al., 2017; García-Pérez et al., 2018; Goumas, 2006;

Onal et al., 2008; Papadopoulos et al., 2007; Parasnis, 1952; Whetton et al., 1956) have carried out laboratory measurements in order to determine the bulk densities of the geological formations existing in their study area.

A set of 3 measurements is required to measure the density of hand samples or cores (Parasnis, 1952), which are the W_1 for the weight of the dry specimen measured in air, the W_2 for weight of the saturated specimen measured in air and the W_3 for weight of the saturated specimen measured in the water. More specifically, we can determine the dry bulk density ρ_d, the saturated bulk density ρ_s and the granular one ρ_g with the following equations given that ρ_w is the water density (almost equal to 1 g/cm^3):

$$\rho_d = \frac{W_1}{W_2 - W_3}\rho_w \quad \rho_s = \frac{W_2}{W_2 - W_3}\rho_w \quad \rho_g = \frac{W_1}{W_1 - W_3}\rho_w$$

Near the surface and especially above the water table the appropriate density is usually the dry bulk one, while the saturated bulk one is more appropriate for larger depths. According to Parasnis (1952), the "field" density is somewhere between the dry and saturated one.

For reliable determination of the densities, it is necessary to measure numerous samples of each geological formation, collected from several locations in order to calculate their average value that will provide a representative value of the formation. It is preferred that the samples are taken from borehole cores since they are more characteristic than the weathered samples from surface outcrops. Nevertheless, for formations that consist of various lithologies, we have to take into consideration the densities of all lithologies for the average ones of the formation itself, but even then, we might not be able to obtain a characteristic density of the formation.

In the framework of this research, laboratory density measurements were carried out on 364 geological specimens (surface outcrops and boreholes cores), collected from several locations of almost every formation existing in Athens basin (Fig. 2). The precision scale used had a readability of 0.001 g.

Beyond our own laboratory measurements of samples and cores gathered by the authors, bibliographic references have also been collected (Table 1), regarding older density calculations from laboratory measurements in the Athens basin (Goumas, 2006; Papadopoulos et al., 2007; Sabatakakis, 1991).

Additionally, according to published literature, several researchers (Ali and Whiteley, 1981; Fernandez-Cordoba et al., 2017; Goumas, 2006; Karastathis et al., 2010; Parasnis, 1952) have carried out measurements based on the Nettleton method (Nettleton, 1939) in order to determine successfully the bulk density of the studied geological formations. This method requires the execution of a profile of closely spaced gravity measurements across a preferably gentle topographic relief (hill or valley), formed by a geological formation, with no lateral variations.

Within the scope of this paper, totally 40 density profiles (Fig. 2) were carried out, constituted of 315 gravity stations. During the data reduction procedure, different values of densities have to be assumed for the calculation of the Complete Bouguer Anomaly along these profiles. Subsequently, all these curves are plotted and compared in a common graph in order to identify the one demonstrating the minimum correlation with the topography. The minimum correlation curve, that gives the estimate of the density of the formation beneath the hill, was identified with the aid of the correlation coefficient formula in worksheets and not just by visual inspection. The assigned values of density ranged from 1.4 to 3.2 g/cm^3 (Fig. 3), with reduced curves produced for every 0.05 g/cm^3.

It is also known that the density of a geological formation is also related to its seismic velocity. Many researchers (Ammirati et al., 2018; Berrocal et al., 2004; Chaubey et al., 2002; Makris and Yegorova, 2006; Makris et al., 2013; Nakada et al., 2002; Sanchez-Rojas and Palma, 2014) have taken advantage of the empirical curves of density-velocity correlation in order to estimate the densities of several geological formations.

We will estimate the density of geological formations, based on published seismic velocity data regarding the Athens basin area. In Table 2, we can observe the densities derived by using three different empirical curves (Brocher, 2005; Gardner et al., 1974; Nafe and Drake, 1961). The majority of the provided velocities for Athens formation come from Louis et al. (2002b), who carried out in-situ measurements on geological outcrops of *Ano Liosia* area. Afterwards, Symeonidis et al. (2005) executed refraction and surface waves tests above a borehole with known stratigraphy at *Glyfada* area. Additionally, Papadopoulos et al. (2001) conducted seismic tomography across boreholes with known stratigraphy at *Kalogreza* area searching for underground cavities. Finally, Papadopoulos et al. (2007) executed three long seismic refraction lines, across the Athens and Thriassio basin, illustrating their results. By checking the surface formations along these profiles and their near-surface seismic velocities, we managed to derive similar velocities to Louis et al. (2002b) for the Triassic-Jurassic Limestones (*T-J*) and the Talus Cones & Scree (*Pt.sc*).

Other authors in the past (Hammer, 1950; Parasnis, 1952; Whetton et al., 1956) tried to define the rock densities by carrying out both laboratory measurements on specimens or cores and survey methods such as the Nettleton profiles. Although Parasnis (1952) declared that laboratory measurements would be sufficiently accurate, he ended up adopting values that were the mean value of the two methods (laboratory measurements and density profiles). On the contrary, Hammer (1950) supported the idea that the density determination can improve with the density profiles rather than by laboratory measurements on specimens. Similar aspects are also presented by Whetton et al. (1956). The last two papers supported that the differences between the two methods can be associated with changes in saturation or mechanical changes during the drilling.

3.2. Results of density determination

As it is illustrated in Table 2, the average densities for all the cohesive lithologies have been calculated. For the majority of the post-alpine sediments covering the Athens basin, we were able to calculate discrete densities for the cohesive lithologies of the formations. The comparison of the bibliographic densities (Table 1) with the ones derived in the framework of this paper (Table 2), reveal that generally all the values are pretty close, except for the *Schists* and *Athens Schists*, where we can observe greater differences. Taking into account that the *Athens Schists* are observed in a form of tectonic mélange, this might explain the differences compered to the literature values, given also the fact that we had several samples of this formation originated from borehole cores.

Furthermore, almost all the geological formations of Athens basin were investigated and their bulk densities were estimated based on the Nettleton method (Table 2). Unfortunately, the results of some profiles were not helpful and therefore were not included in the evaluation. The reason of these profiles being misrepresentative was probably due to their locations (not in the interior of the basin), close to mountain slopes and therefore influenced by the intense regional field. Unfortunately, the locations for planning and executing such density profiles were very limited.

Finally, the density values calculated from the published seismic velocity data are quite smaller than both the laboratory measurements and the Nettleton profiles, especially for the Triassic-Jurassic Limestones and the Volcanosedimentary sequence. However, important density values for relatively uncohesive lithologies have been calculated, such as the Loose Quaternary deposits (*Q-Al*), the conglomerates and clays, for which we could not execute Nettleton profiles.

It is also important to notice that for some of the geological formations/lithologies of Athens basin, such as the Marbles (*M*), the Schists

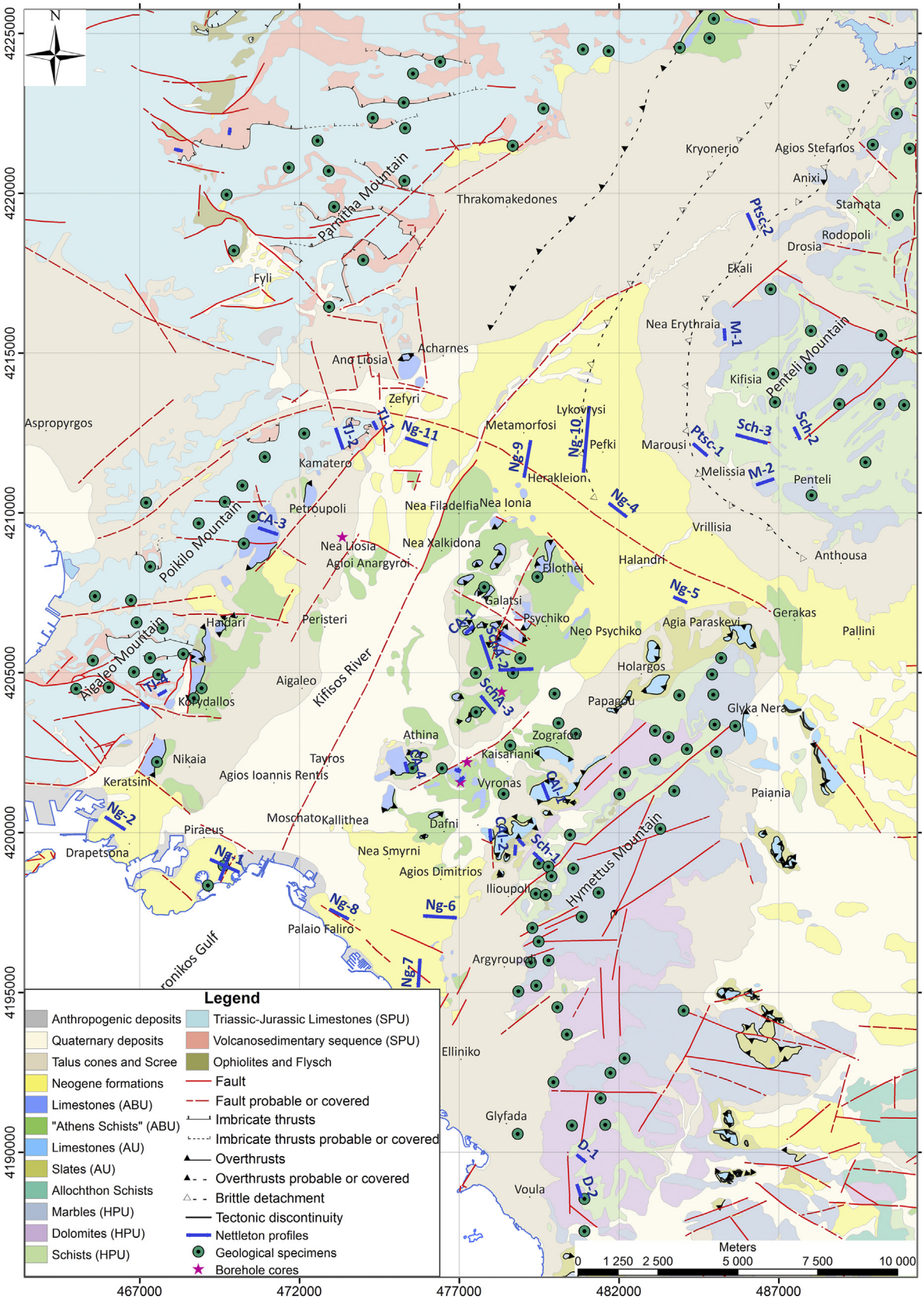

Fig. 2. Locations of geological specimens and borehole cores measured for density. The Nettleton profiles are also illustrated.

Table 1
Bibliographic densities for geological formations/lithologies of Athens basin.

Geological formation/lithology	Papadopoulos et al., 2007. (ρ_d in gr/cm^3)	Sabatakakis, 1991 (ρ_d in gr/cm^3)	Goumas, 2006 (ρ_d in gr/cm^3)
Triassic-Jurassic Limestones (*T-J*)	2.72 ± 0.01	2.68	2.72 ± 0.04
Marbles (*M*)	2.69 ± 0.01	2.88	–
Schists (*Sch-Penteli Mt.*)	2.81 ± 0.05	2.78	–
Volcanosedimentary sequence (*C—P*)	2.57 ± 0.03	–	–
Athens Schists (*SchA*)	2.65 ± 0.02	2.51	–
Limestones of Athens Basin Unit (*CA*)	–	2.68	–
Marls	2.01	2.07	–
Conglomerates	2.42	2.44	2.46 ± 0.10
Marly Limestones	–	2.4–2.62	–

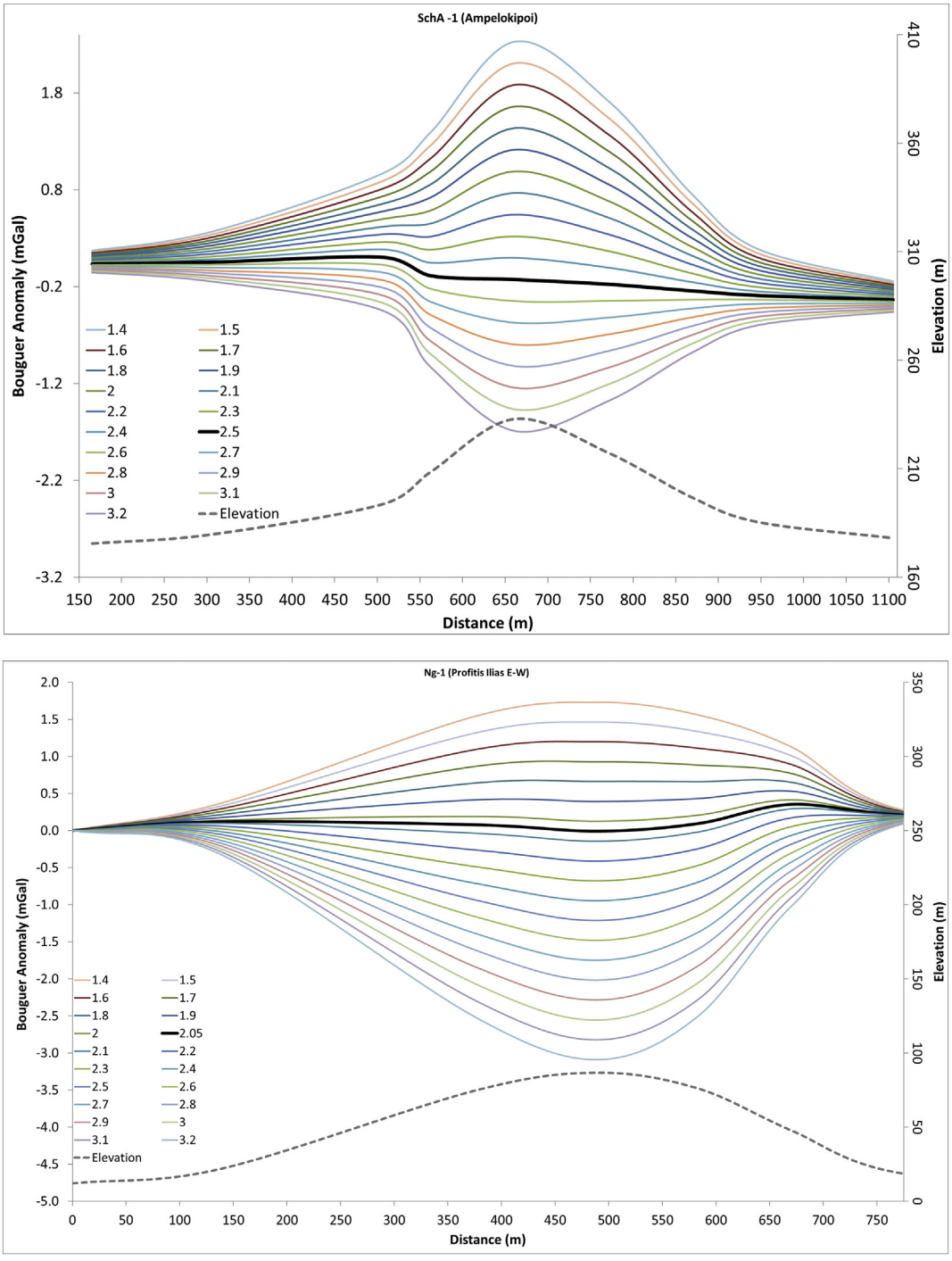

Fig. 3. Examples of Nettleton profiles for geological formations of the Athens basin. The upper profile is located in the central part of Athens basin (*Ampelokipoi*) and the lower one at the southwestern part, at *Piraeus*.

Table 2
Average densities of the geological formations or individual lithologies in Athens basin, derived from a) the laboratory measurements of hand samples and borehole cores (blue cells), b) the application of Nettleton (1939) profile method (green cells) c) the empirical curves of velocity-density correlation (orange cells), based on by 1: in-situ measurements (Louis et al., 2002b), 2: Refraction data (Symeonidis et al., 2005) and 3: Cross-hole data (Papadopoulos et al., 2001). All the provided densities are in gr/cm^3.

Geological formation/lithology	Laboratory measurements				Nettleton method		Velocity-density correlation			
	Number of Specimens	Dry bulk density ρ_d	Saturated bulk density ρ_s	Grain density ρ_g	Density profiles	Density (gr/cm^3)	V_p (in m/s)	Density by Gardner *et al.*	Density by Nafe & Drake	Density by Brocher
Triassic-Jurassic Limestones (*T-J*)	60	2.66 ±0.04	2.68 ±0.04	2.70 ±0.04	4	2.55-2.65	3,500-4,500	2.38-2.54	2.32-2.46	2.32-2.48
Dolomites (*D*)	20	2.74 ±0.07	2.76 ±0.07	2.79 ±0.07	2	2.60	-	-	-	-
Marbles (*M*)	30	2.66 ±0.02	2.68 ±0.03	2.71 ±0.04	2	2.60	-	-	-	-
Schists (*Sch-Hymettus Mt.*)	11	2.43 ±0.05	2.54 ±0.03	2.76 ±0.02	1	2.55	-	-	-	-
Schists (*Sch-Penteli Mt.*)	5	2.57 ±0.05	2.68 ±0.10	2.94 ±0.29	2	2.75	-	-	-	-
Volcanosedimentary sequence (*C-P*)	16	2.51 ±0.05	2.57 ±0.03	2.67 ±0.03	2	2.35-2.45	2,300	2.14	2.03	2.05
Limestones Athens Basin Unit (*CA*)	28	2.64 ±0.04	2.66 ±0.03	2.70 ±0.02	7	2.50-2.55	-	-	-	-
Limestones of Alepovouni (*CAl*)	21	2.64 ±0.04	2.66 ±0.02	2.70 ±0.01	2	2.65	-	-	-	-
Athens Schists (*SchA*)	38	2.55 ±0.07	2.60 ±0.05	2.69 ±0.05	3	2.50-2.55	-	-	-	-
Slates of Alepovouni (*Sch-Al*)	13	2.19 ±0.09	2.36 ±0.08	2.61 ±0.10	2	2.55	-	-	-	-
Limestones (*Ng-Plm*)	5	2.55 ±0.04	2.59 ±0.05	2.67 ±0.07	11	1.95-2.15 & 2.40	1,400-1,600	1.90-1.96	1.6-1.70	1.6-1.7
Marly limestones (*Ng-Plm*)	12	2.45 ±0.05	2.52 ±0.04	2.63 ±0.02						
Sandy marls (*Ng-Msm*)	18	1.60 ±0.09	1.91 ±0.12	2.36 ±0.24						
Breccia & sand (*Ng-Msm*)	6	2.50 ±0.11	2.55 ±0.07	2.65 ±0.03						
Reddish clays (*Ng-Msl*)	5	2.49 ±0.03	2.56 ±0.03	2.68 ±0.01						
Marls (*Ng-Msl*)	6	1.72 ±0.07	1.96 ±0.14	2.29 ±0.31						
Marly limestones & Sandy marls (*Ng-Msl*)	18	2.13 ±0.16	2.29 ±0.11	2.52 ±0.06						
Clay & Sand (*Ng-Pll*)	5	-	2.16 ±0.04	-						
Talus cones & Scree (*Pt.sc*)	1	2.28	2.39	-	2	-	1,800-1,900	2.02-2.05	1.81-1.86	1.80-1.87
Loose Quaternary deposits (*Q-Al*)[1]	-	-	-	-	-	-	1,100-1,500	<1.93	<1.64	<1.6
Conglomerates[2]	-	-	-	-	-	-	2,080-2,270	2.09-2.14	1.95-2.05	1.94-2.02
Clays[3]	-	-	-	-	-	-	1,000-2,500	<2.19	<2.09	<2.1
Breccia[3]	-	-	-	-	-	-	2,500-3,000	2.19-2.29	2.09-2.22	2.1-2.21
Metabasic	9	3.05 ±0.04	3.10 ±0.03	3.20 ±0.03	-	-	-	-	-	-

(*Sch-Hymettus Mt.*), the Limestones and the Slates of Alepovouni (*CAl and Sch-Al* correspondingly), there was no data at all regarding their densities. In the context of this study, we managed to calculate for the first time their density.

3.3. Adopted densities

In our case, it seems that the application of Nettleton method for determining the density of the Athens formations proved valuable regarding the post-alpine formations (*Ng*), because they were either too unconsolidated to be measured in the laboratory or they were comprised of several different lithologies (Papanikolaou et al., 2002). Each lithology has its own density that was calculated through laboratory measurements but the final representative value of the whole formation could not be estimated given the fact that we were not able to measure the unconsolidated lithologies. The density profiles were equally helpful in the case of the Athens Schists (*SchA*), which are considered to be a mélange.

On the other hand, the most carbonate formations, such as the Triassic-Jurassic limestones (*T-J*), the Dolomites (*D*), the Marbles (*M*) and the Limestones of Athens Basin Unit (*CA*), are characterized by lower densities based on the Nettleton profiles results and are not quite representative. This could be due to the increased weathering (Hammer, 1950; Whetton et al., 1956), existing cavities or due to the regional anomalies (Hammer, 1950), given the fact that the density profiles of the first three (*T-J, D, M*) were carried out constrainedly close to mountain slopes and therefore regional anomalies. The same discordances, probably for similar reasons, are observed for the Volcanosedimentary sequence (*C—P*), the Schists (*Sch*) - mainly for the ones of *Penteli* Mt. - and the Slates of Alepovouni (*Sch—Al*). For all these formations, the adopted densities were based on the laboratory measurements (Table 3).

In the case of the Loose Quaternary deposits (*Q-Al*) the only available density was derived from published seismic velocity data, since it is obvious that no laboratory measurements can be executed. Moreover, the density of the inhomogeneous formation of Talus Cones & Scree (*Pt.sc*) was selected somewhere between the laboratory measurements and the density derived from the seismic data (Table 2), because the Nettleton profiles could not determine a density value.

Table 3
Adopted densities of geological formations, used in gravity data processing of this paper.

Geological formation/lithology	Adopted density (gr/cm^3)	Dominant method	Standard deviation
Triassic-Jurassic Limestones (*T-J*)	2.68	Laboratory	±0.04
Dolomites (*D*)	2.76	Laboratory	±0.07
Marbles (*M*)	2.68	Laboratory	±0.03
Schists (*Sch-Hymettus Mt.*)	2.54	Laboratory	±0.03
Schists (*Sch-Penteli Mt.*)	2.68	Laboratory	±0.10
Volcanosedimentary sequence (*C—P*)	2.57	Laboratory	±0.03
Limestones of Athens Basin Unit (*CA*)	2.66	Laboratory	±0.03
Limestones of Alepovouni (*CAl*)	2.65	Lab & Nettleton	±0.02
Athens Schists (*SchA*)	2.50	Nettleton	±0.05
Slates of Alepovouni (*Sch-Al*)	2.36	Laboratory	±0.08
Neogene formations/Several lithologies (*Ng*)	2.10	Nettleton	±0.05
Talus Cones & Scree (*Pt.sc*)	2.30	Lab & Seismic	±0.10
Loose Quaternary deposits (*Q-Al*)	1.60	Seismic	–

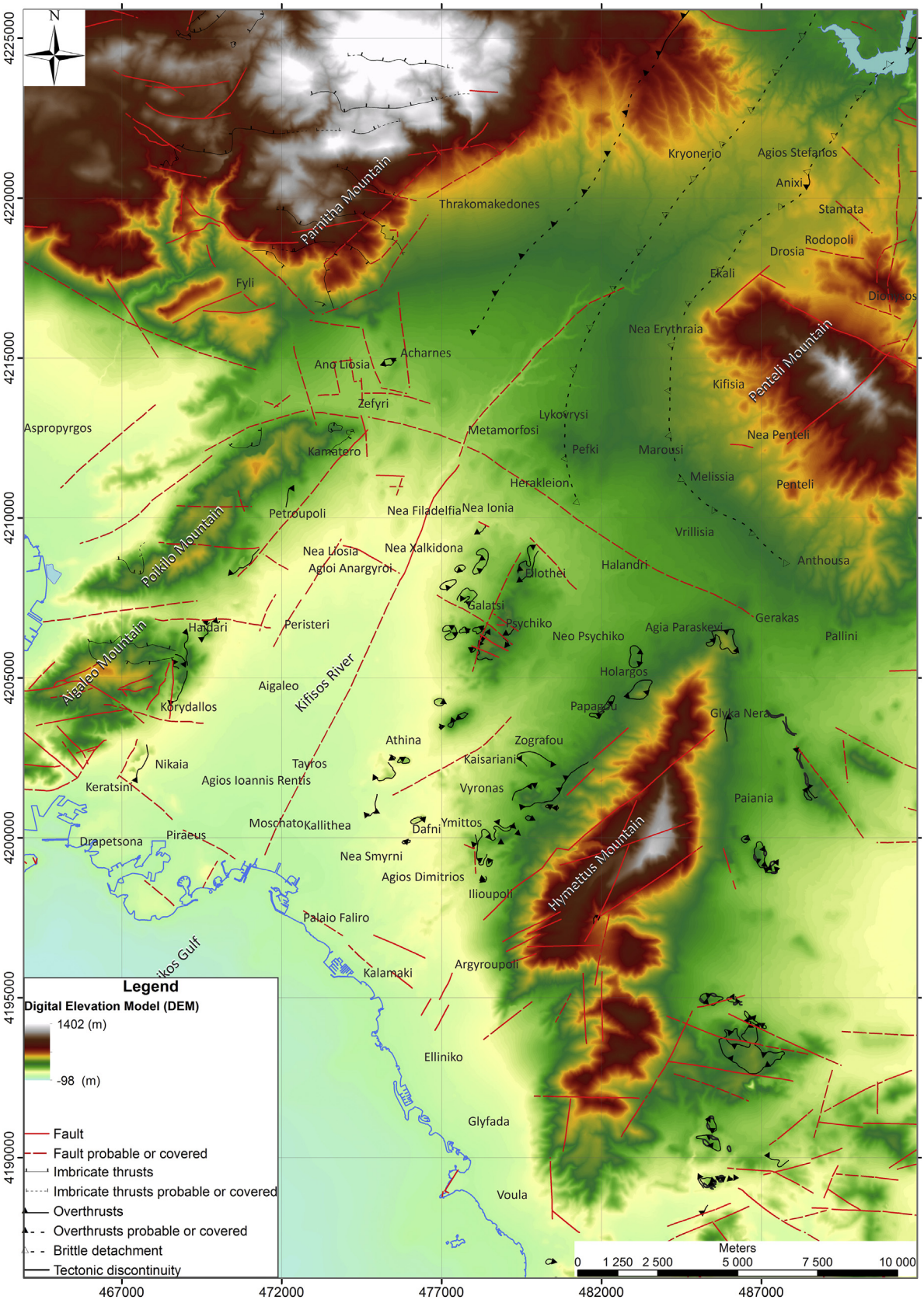

Fig. 4. Digital Elevation Model (DEM) of Athens basin.

The errors of the adopted values for each formation/lithology are also illustrated in Table 3. Taking into account that for the majority of them we have selected the results of the laboratory measurements, we provide their standard deviation. For the densities selected from Nettleton profiles, we provide the standard deviation among all the profiles of each formation. The authors

believe that the errors are small and thus the adopted values acceptable.

4. Gravity survey

4.1. Acquisition

A gravity base network of thirteen (13) bases was established (Dilalos, 2018) for the purpose of this study. The entire gravity base network is referred to the IGSN'71 datum (Morelli et al., 1974) as it was tied with repeated measurements with an already established base in the University of Athens (Hipkin et al., 1988). Due to the complicated geology of the area, the purpose of the research and the urban environment, the gravity measurements were organized on a grid and not on a few profiles. The grid station spacing had been set primarily to 1 km. After the processing of the first dataset, the grid became a little denser, with some stations added in between the first ones, in order to clarify the status in some areas. The gravity database comprised of 1.122 gravity stations (Fig. 1), of which the 315 have been collected along Nettleton profiles acquired during the summers of 2013 and 2014. The gravity meter LaCoste & Romberg G-496 was used for the data acquisition .

In order to calculate the necessary coordinates of each gravity station and base with high precision, we used Differential Global Positioning System (dGPS). In this way, the accuracy of the calculated coordinates was limited to a few centimeters, which is very important in order to have precise data corrections and results. The coordinates were calculated in the Hellenic Geodetic Reference System (EGSA'87).

4.2. Data reduction

The drift correction and the tidal effects were removed with the *Oasis Montaj* software, based on the measurement time of each station. The next step includes the latitude (*WGS84 formula*) and free-air correction, where the calculated coordinates of each gravity station are taken into account. The assumed constant density for the Bouguer correction was set up to 2.67 g/cm^3. At this point, the Simple Bouguer Anomaly has been calculated (Dilalos, 2018; Dilalos and Alexopoulos, 2017).

In order to calculate the necessary terrain correction, we used an accurate Digital Elevation Model (DEM), Fig. 4. In this paper, we used the *Gravity and Terrain Correction* extension of *Oasis Montaj* for the terrain correction calculation. An inner radius equal to 1.500 m had been set, along with an outer radius distance equal to 21 km. Normally, with the aim of calculating the Complete Bouguer Anomaly only the Terrain corrections need to be added to the Simple Bouguer Anomaly. However, in this urban geophysical survey, we have also to calculate and add the Building Correction (Dilalos, 2018; Dilalos et al., 2018), caused by the building and infrastructures of the city. The values of the Complete Bouguer Anomaly (Fig. 5) range from 34 up to 79.0 mGal. An area of minimum values, with circular shape, is located in the northern suburbs, among the areas of *Thrakomakedones*, *Kryoneri*, *Ekali*, *Kifisia*, *Lykovrysi* and *Acharnes*. The Bouguer values seem to be increasing to the southern areas and especially over the mountain Hymettus where the maximum values exist. Finally, the local residual anomaly maps have also been produced through the application of Fourier Filtering that was based on the energy spectrum of the data (Dilalos, 2018).

4.3. Regional-residual separation

In the context of this paper, we chose to proceed to the regional-residual separation with Fourier analysis and Filtering (Anudu et al., 2016; Dilalos and Alexopoulos, 2017; Elkhodary and Youssef, 2013; Khamies and El-Tarras, 2010). The processing was carried out with the contribution of Oasis Montaj software and the *MAGMAP* extension, since the measurements were executed on a grid plan.

The separation of the regional and residual gravity fields was based on the information provided by the corresponding Power Spectrum Analysis (Fig. 6) of the Complete Bouguer data, which is a common procedure executed before the Fourier filtering (Al-Banna and Al-Karadaghi, 2018; Ali et al., 2017; Elkhodary and Youssef, 2013; Fernandez-Cordoba et al., 2017; Gabtni and Jallouli, 2017; Khamies and El-Tarras, 2010). The power spectrum, calculated by averaging all the grid elements at the wavenumber, can provide depth estimates of the anomaly sources (h), based on the relation h = S/4π, introduced by Spector and Grant (1970) for aeromagnetic data, where S is the slope of the least-squares line of each section of the spectrum.

After several tests with the provided filters, the application of the Gaussian filter, which has successfully applied in several other cases (Anudu et al., 2016; de Castro et al., 2014; Damaceno et al., 2017; Dilalos and Alexopoulos, 2017; Fernandez-Cordoba et al., 2017) has been chosen. The calculation for the residual field is derived from the following formula:

$$L_{(k)} = 1 - e^{\frac{-k^2}{2k_0^2}}$$

where k_0 is the standard deviation of the Gaussian function in cycles/ground unit, applying it as a smooth high-pass filter. Based on the above results of the power spectrum (Fig. 6), we produced a residual map with a cutoff wavelength of 500 m and standard deviation equal to 0.25 cycles/km (Fig. 7) revealing mostly the shallow structures. Beyond that, a second residual map of the basement, with standard deviation equal to 0.02 cycles/km, was produced (Fig. 8), including also the anomaly sources and information from deeper structures of the bedrock.

Starting from the residual map of the basement (Fig. 8), its values range from −15.2 mGal to 9.4 mGal, with the contribution of both deep and shallow structures. We can observe two areas of minimum values (down to −15.2 mGal). The main one is located in the northern part of the study area, with relatively circular shape, along with two linear extensions, one extending to southernwest and another to northeastern. A second area of minimum values is located southern, almost parallel to the urban coastline, reaching a minimum anomaly value of −6.5 mGal.

On the other hand, the maximum anomaly values are observed at the areas of the surrounding mountains *Hymettus* (up to 9.4 mGal), *Aigaleo-Poikilo* (up to 2.5–3 mGal) and *Parnitha* (up to 2–4 mGal). Moreover, an area of the inner basin appears with a maximum positive anomaly value of almost 2.7 mGal, located in the central-western area. The general direction of this zone (WNW-ESE) is almost perpendicular to the general direction of the mountains *Hymettus* and *Aigaleo* (NNE-SSW).

Going up to the shallow anomaly sources and structures (Fig. 7), the values of the residual map range from −1.82 mGal to 1.51 mGal. Structures of high and low values of gravity are alternating, especially in the western area. The low gravity area (down to −0.9 mGal) at the northern part is spatially constrained relatively to the image of the basement residual (Fig. 8), surrounded by a zone of high gravity from west and north (southern foothills of *Parnitha Mt.*) with values up to almost 1 mGal. A big linear zone of low gravity (down to −1.5 mGal) has been revealed running across the western suburbs ending up southern to the area of *Piraeus*. This zone is laterally constrained by two other linear zones of higher gravity (up to almost 1 mGal) with similar direction.

4.4. Structural mapping

After the separation of the gravity field into residual and regional components, we can take advantage of the derivatives methods in order to enhance the structural edges. The structural mapping is very common in the scientific literature the latest years and has been very helpful in structural investigations (Ali et al., 2017; Anudu et al., 2016;

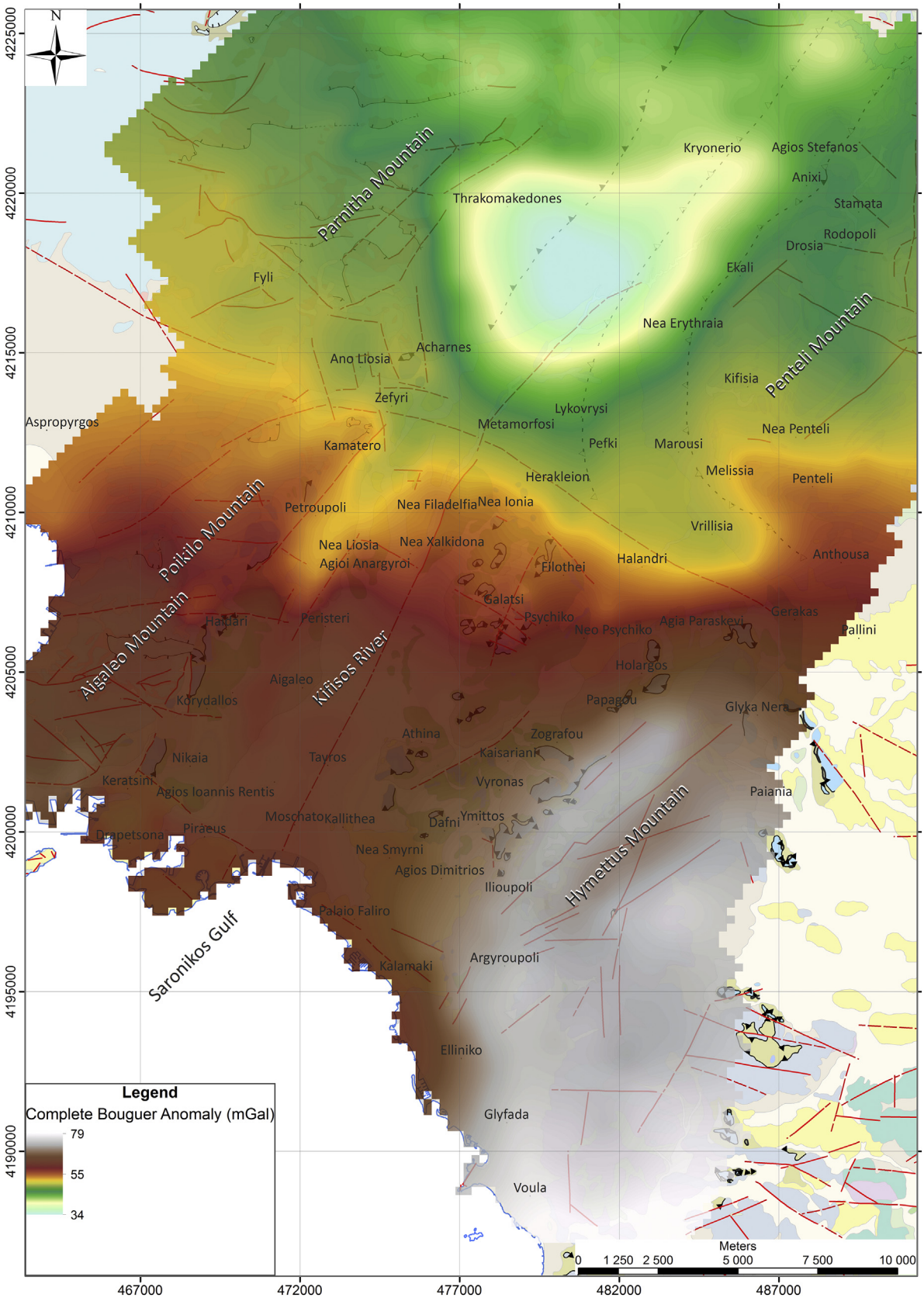

Fig. 5. Complete bouguer anomaly map of Athens basin.

Cooper and Cowan, 2008; Elkhodary and Youssef, 2013; Eshaghzadeh, 2015; Ghosh, 2016; Hosseini et al., 2013; Khalil et al., 2015; Khamies and El-Tarras, 2010; Koumetio et al., 2012; Martins-Ferreira et al., 2018; Nasuti et al., 2012; Wu et al., 2017). For that reason, we proceeded to this method in order to outline the structural edges of Athens basin using Oasis Montaj software.

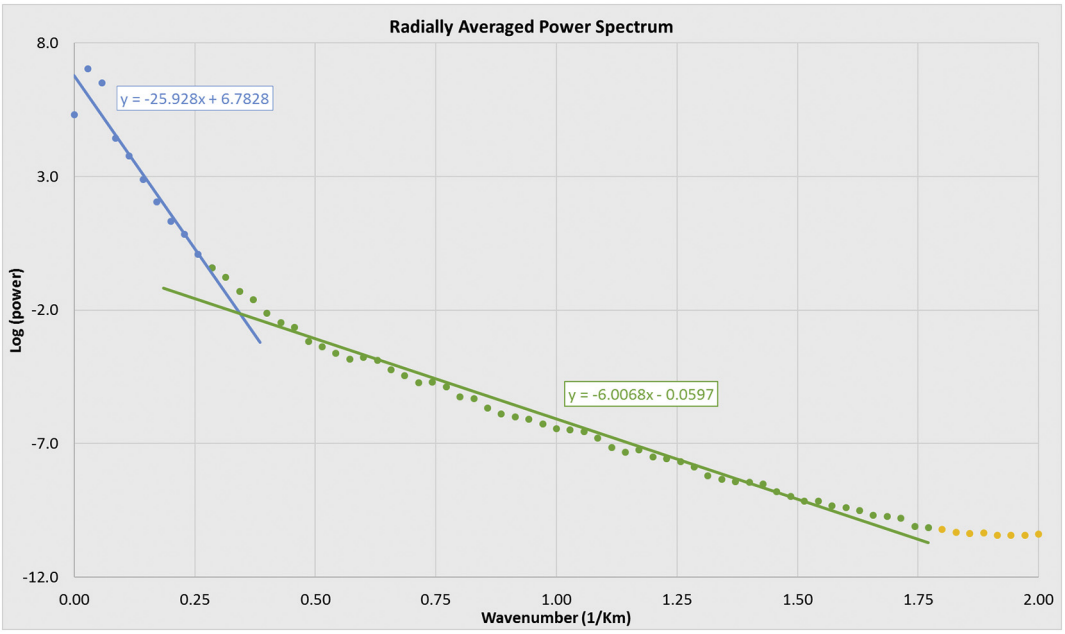

Fig. 6. Radially averaged power spectrum of the complete bouguer anomaly of Athens basin.

There are several methods using the derivatives that can provide the desired enhancement of the structural edges. Based on Fairhead (2015), the traditional ones are the amplitude derivatives, such as the Total Horizontal Derivative (THDR), the First Vertical Derivative (VDR), the Second Vertical Derivative (SVDR) and the Analytical Signal (AS). They are directly related and controlled by the lateral variation in density of the source bodies and therefore with the geology. On the other hand, we also have the local phase derivatives, such as the Tilt (Tilt) and the Theta (cos Tilt), which are independent of density.

In the context of this paper, we applied most of the aforementioned edge enhancement techniques. Firstly, the results of the Total Horizontal Derivative (THDR) are illustrated in Fig. 9 for the shallow sources and in Fig. 10 for the deeper ones. The maximum values identify linear edges such as fault zones and contacts, especially for shallow structures, identifying large and small edges with large and small density contrasts (Fairhead, 2015). The THDR results for the shallow structures (Fig. 9), reveal three linear zones of maxima with general direction NE-SW. The major one extends from the area of *Piraeus*, *Nikaia*, *Aigaleo*, *Agioi Anargyroi*, *Zefyri* and ends up to *Thrakomakedones*. One other zone is observed along the axis of the central hills (*Filopappou*, *Lycabettus*, *Attiko Alsos*, *Tourkovounia*) and one along the western part of the *Hymettus* Mountain. Smaller maxima are also located along the area of *Kalamaki-Elliniko* and *Kryoneri-Agios Stefanos*. The same image, but more intense, is observed for the results of the basement sources (Fig. 10). The area among *Thrakomakedones*, *Ekali*, *Nea Erythraia* and *Acharnes* presents wider areas of maxima and so does the one of *Agia Paraskevi* and *Papagou*.

The results of the First Vertical Derivative (VDR) are illustrated in Fig. 11 (shallow structures) and Fig. 12 (basement structures). This technique is also more sensitive to the shallow structures (Fairhead, 2015). Parts of the zero crossing adumbrate the edge location while the maxima values outline the structure location providing simultaneously information about its positive or negative density and therefore for its dip. The negative values of the derivative have been removed in an effort to manage it more easily (Fairhead, 2015) by illustrating only the structural edges (zero crossings) and the positive structures-possible horsts only (maxima). The removal of the negative values has also been presented by other authors (Ali et al., 2017; Nasuti et al., 2012) for the construction of Tilt maps, which adumbrate the edges in a similar way (zero crossings).

The results of the VDR (Figs. 11–12) indicate almost the same edges as those of the THDR (Figs. 9–10), but providing also information about the relative block position (positive density bodies). However, in two areas it seems to clarify a little bit more the structural status. One of them is the western and southern part of *Penteli* Mountain and the other one is the western part of *Hymettus* Mountain, where strong indications reveal the existence of great structural edges. These maxima (positive structures-horsts) run along the same areas for both shallow and basement structures.

The last amplitude derivative applied in Athens basin was the Analytic Signal (AS), observed in Fig. 13 (shallow structures) and Fig. 14 (basement structures). Practically, the maximum values outline the edges that THDR have also done and especially for the zone of the eastern foothills of *Aigaleo-Poikilo* and *Parnitha* Mountains. It also delineated similar zones with THDR on *Hymettus* Mountain and along the axis of hills in the basin interior. The produced Analytic Signal maps (Figs. 13–14) seem a little noisier, compared to that of THDR (Figs. 9–10).

Following this we move on to the application of the phase derivatives, by first calculating the Tilt derivative (Figs. 15–16), at which the zero crossing lines are related to the location of the structural edges and the maxima delineate the positive density structures (possible horsts). The results for both shallow and deeper structures reveal an almost identical image with the corresponding VDR maps (Figs. 11–12), with the same zones adumbrated but slightly more definite. The main difference between the two derivatives is that the *Tilt* one is independent of the density and relatively smoother. It also prevents the domination of the large density contrast edges (Fairhead, 2015).

Finally, the Theta derivative has been calculated based on the *Tilt* and is illustrated in Fig. 17 (shallow structures) and Fig. 18 (basement structures). Taking into account that it is practically the cosine of *Tilt* derivative, its maximum values ($\approx$1) will delineate the structural edges. In the produced *Theta* maps of Athens basin (Figs. 17–18) we have isolated the values >0.8 (the units are in radians), trying to produce more perspicuous images, with obvious linear structures, normally related to the structural edges. The *Theta* map for the shallow structures (Fig. 17) reveals exceptionally limited areas, regarding the results of all the derivatives applied. The map of the deeper bodies (Fig. 18) clearly shows the edges, which practically are identical with those of the prementioned structural maps.

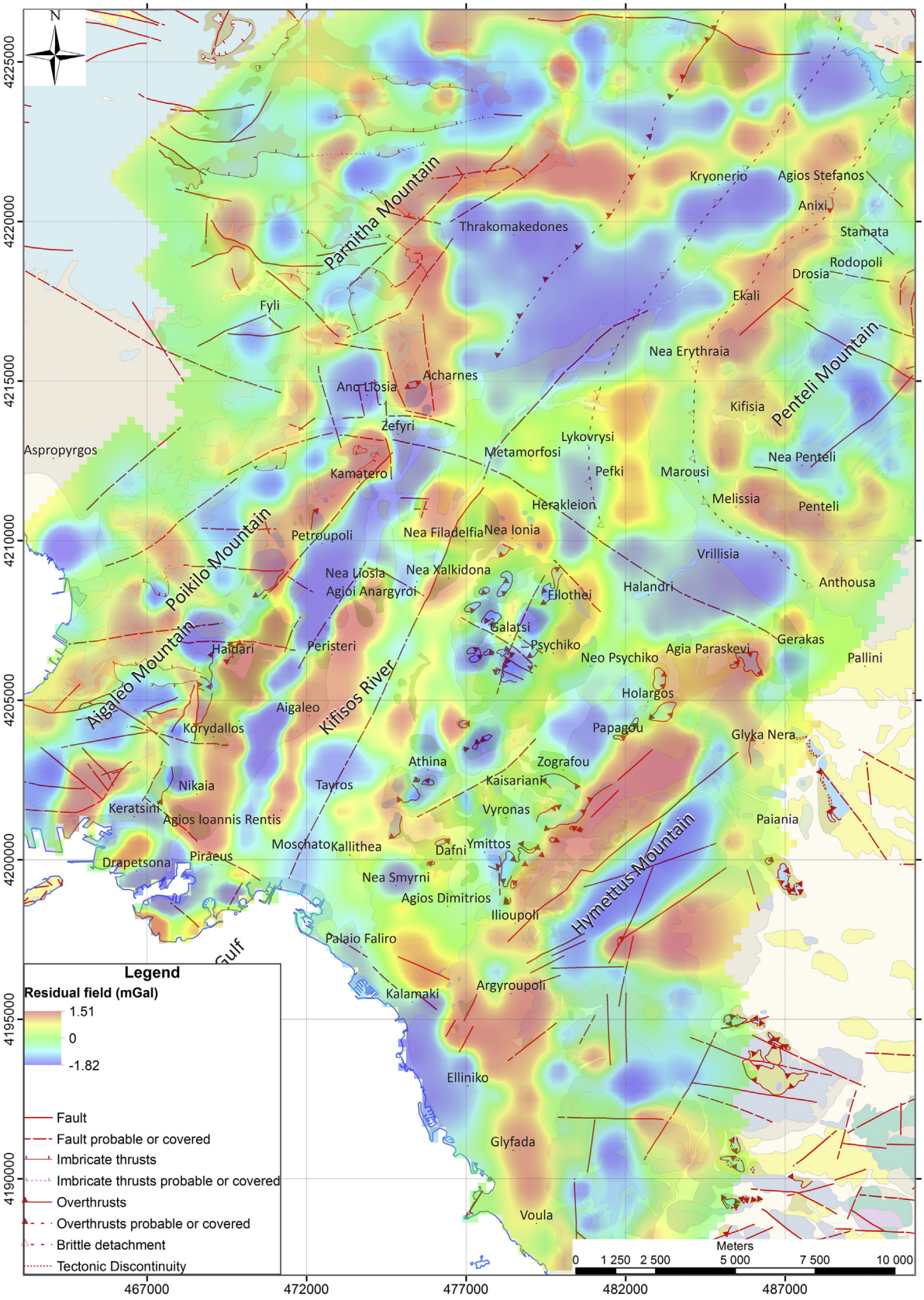

Fig. 7. Residual map of Athens basin with standard deviation equal to 0.25 cycles/km, illustrating the shallow anomaly sources.

The southern part of the major fault zone of *Kifisos*, from *Agioi Anargyroi* to *Faliro*, seems to have been verified. The VDR (Fig. 11) and *Tilt* (Fig. 15) maps of the shallow sources, illustrate an area corresponding to a graben structure, since structural edges have been revealed edgeways. One of these two edge zones could be recognized as the *Kifisos* zone, but slightly shifted eastwards. This can also be

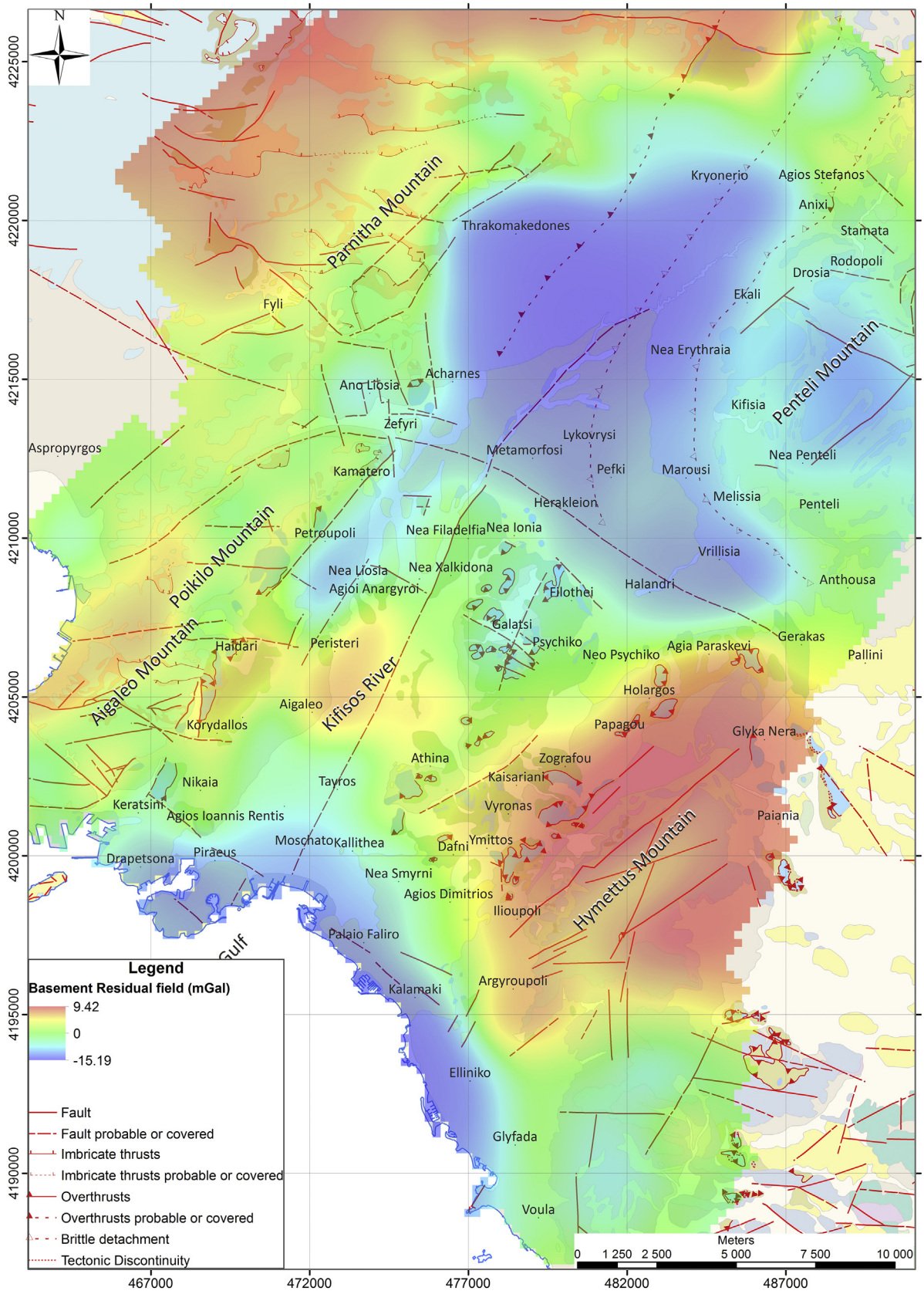

Fig. 8. Residual map of basement with filter standard deviation equal to 0.02 cycles/km, illustrating the deeper bedrock anomaly sources.

confirmed by the low areas of the THDR (Fig. 9). The already mapped part of the *Kifisos* zone, from *Agioi* Anargyroi to Nea *Filadelfia*, has been partially revealed in the VDR (Fig. 11), Tilt (Fig. 15) and AS (Fig. 13) maps. Moreover, the probable extension of *Kifisos* to the north (*Metamorfosi-Lykovrysi-Nea Erythraia*) might have been adumbrated only partially at the *Metamorfosi* area by the shallow VDR (Fig. 11)

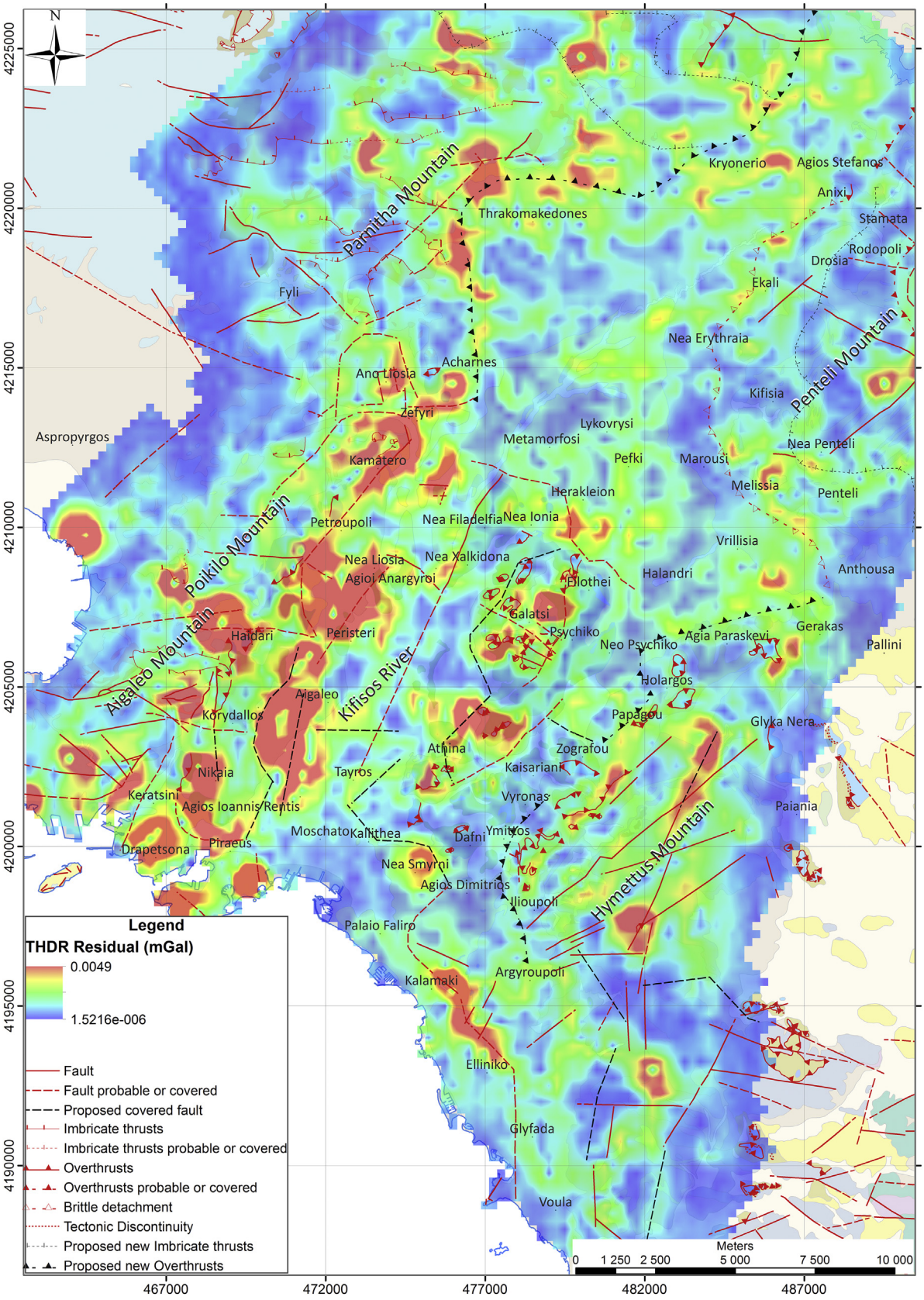

Fig. 9. THDR of residual data (shallow structures).

and Tilt (Fig. 15) maps. The THDR (Fig. 10) and Analytical Signal (Fig. 14) maps of the deeper bodies seem to indicate its northern extension to *Nea Erythraia* but in quite bigger depths.

Likewise, for the other major probable zone with direction almost E-W (*Zefyri-Agia Paraskevi*), we have systematic indications presented in almost all the derivative maps, but not for its total length. Therefore,

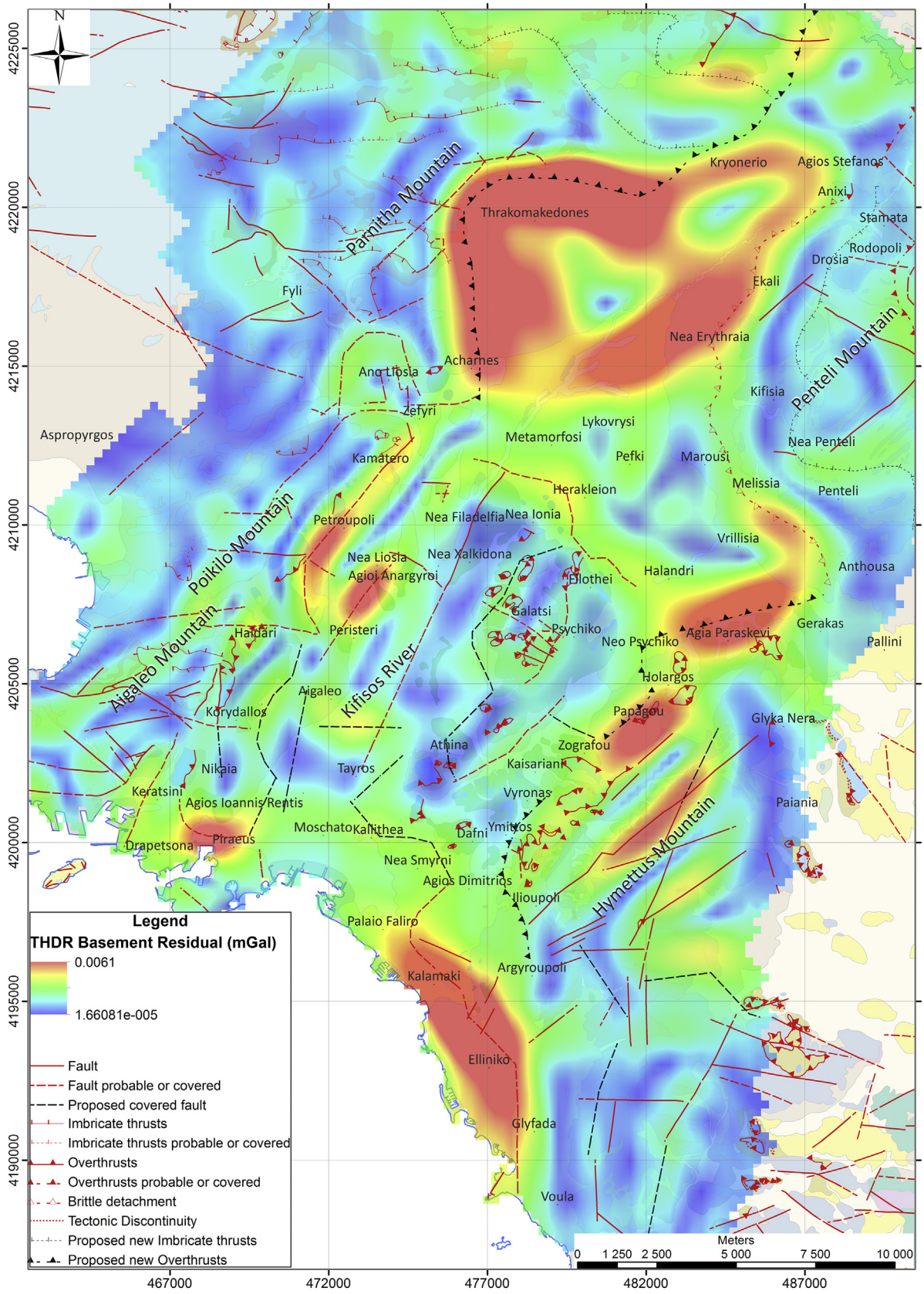

Fig. 10. THDR of residual data (deep structures).

we can verify its central section along *Metamorfosi- Herakleion -Halandri*, its western edge at *Zefyri* and its eastern one at *Agia Paraskevi-Gerakas*. Its probable extension to the west and southwest is confirmed only at the northwest foothills of *Poikilo* Mt. (*Homateri* area), but no indications have been revealed for its farther extension to *Neoktista* and *Koumoundourou Lake*.

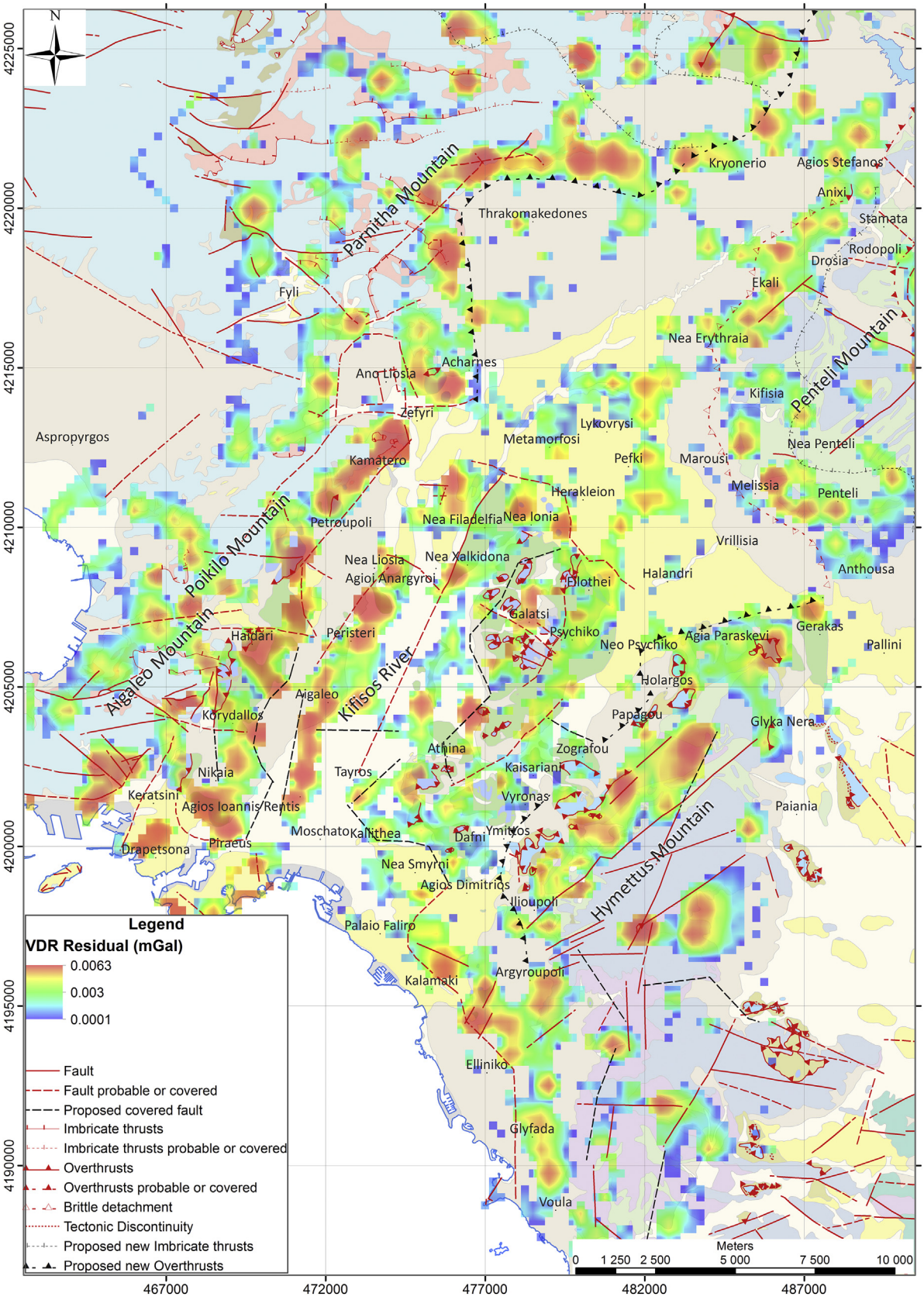

Fig. 11. VDR of residual data (shallow structures).

Beyond these, we have strong indications verifying the overthrust of the brittle detachment, which was characterized as probable. This zone runs around the western and southern foothills of *Penteli* Mt., along *Agios Stefanos*, *Ekali*, *Nea Erythraia*, *Melissia*, *Penteli* and *Anthousa* and has been revealed in most of the structural maps. Especially in the VDR (Figs. 11–12) and *Tilt*

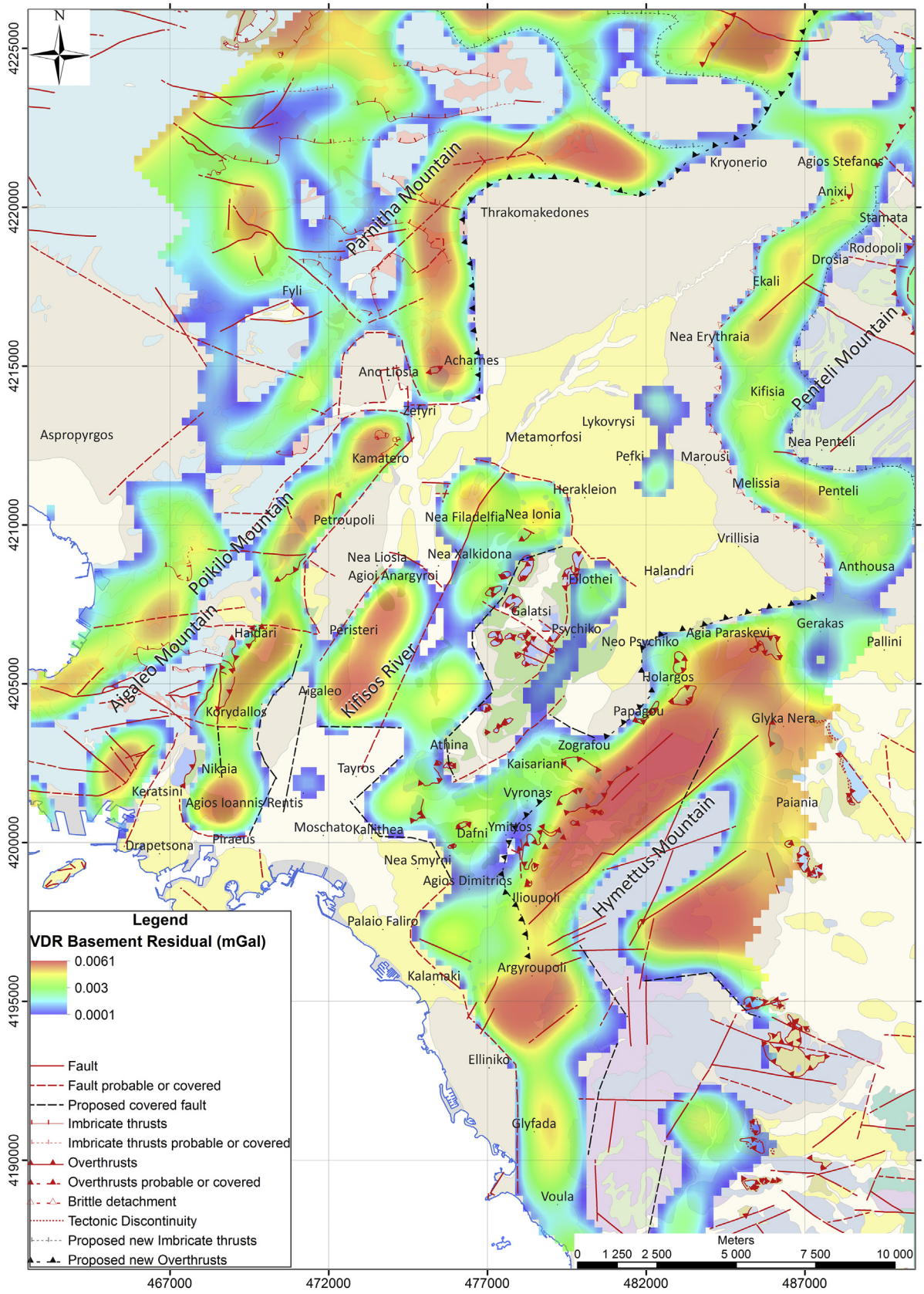

Fig. 12. VDR of residual data (deep structures).

(Figs. 15–16) maps, an edge zone is presented almost with identical trace with the zone already proposed as an Upper Cretaceous overthrust. The delineation is more obvious at the results derived from the basement data. Concerning the other proposed Upper Cretaceous overthrust, located west of the prementioned one, only the section along the areas of *Lykovrysi-Peyki* can be also

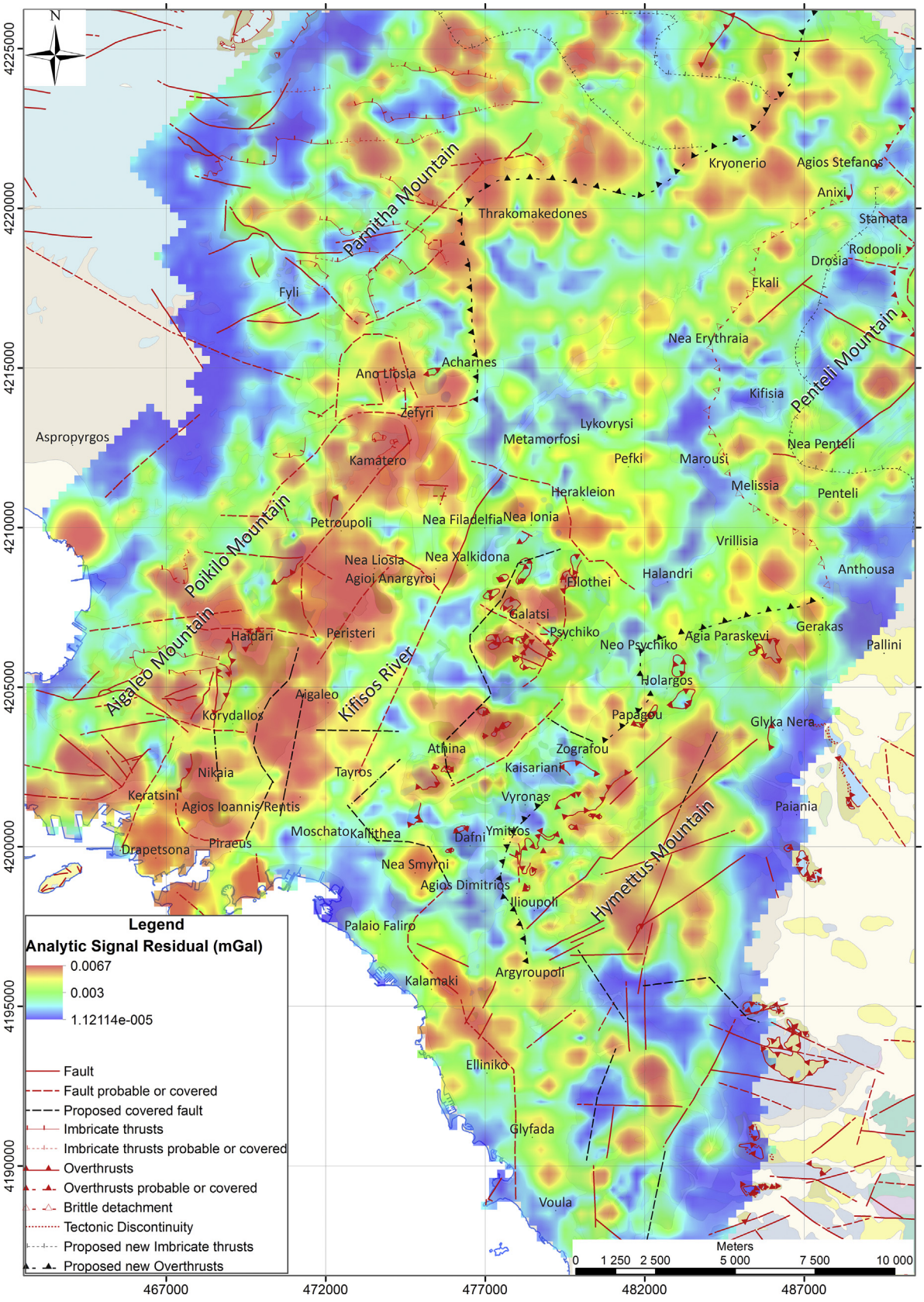

Fig. 13. Analytic signal of residual data (shallow structures).

observed in the derivative maps. Of course, apart from the confirmation of several mapped faults (visible or covered), the structural mapping based on the derivatives has revealed several more locations of probable fault zones or contacts, which have not been proposed yet. There are some linear features that could easily match to faults or contacts. Some of these are along

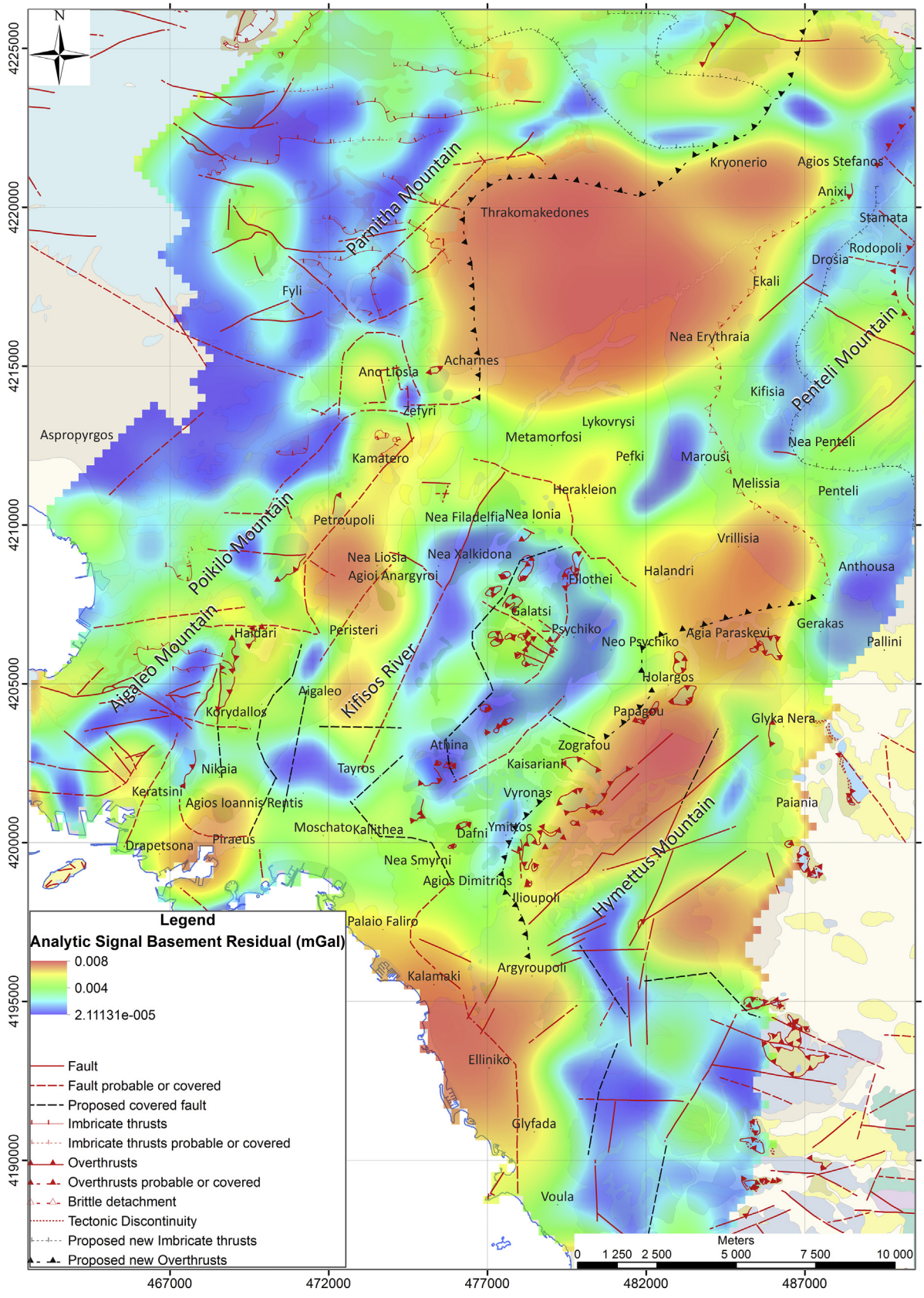

Fig. 14. Analytic signal of residual data (deep structures).

Nikaia-Korydallos, *Piraeus-Agia Varvara*, *Agios Ioannis Rentis-Aigaleo-Peristeri*, *Kalamaki-Elliniko-Glyfada*, *Nea Smyrni-Agios Dimitrios*, *Zografou-NeoPsychiko-Filothei*, *Thrakomakedones-Kryoneri-Agios Stefanos*, *Lycabettus-Strefi* hills and *Drapetsona*. Most of them could be characterized as prolongations of adjacent mapped (visible or probable) structural edges.

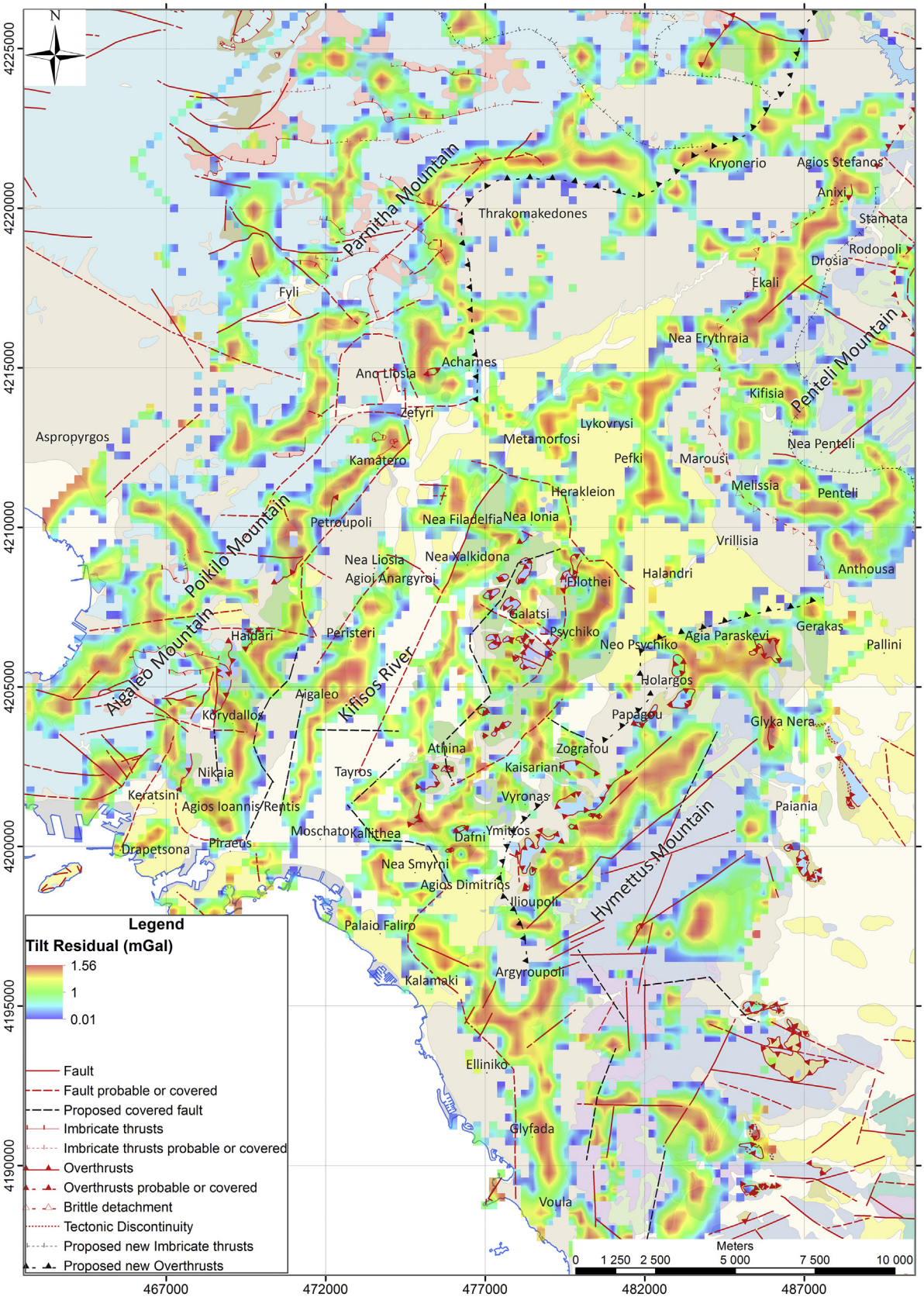

Fig. 15. Tilt derivative of residual data (shallow structures).

Finally, one more major structural edge has been detected by most of the derivative maps and is clearly presented in the VDR (Figs. 11–12) and Tilt (Figs. 15–16). This zone is observed at the east foothills of Hymettus Mt., along the areas of *Gerakas*, *Agia Paraskevi*, *Holargos*, *Papagou*, *Zografou*, *Vyronas*, *Kareas*, *Ilioupoli*, *Argyroupoli*, Glyfada and *Voula*. The detachment between the *Hymettus-Penteli Unit* and the

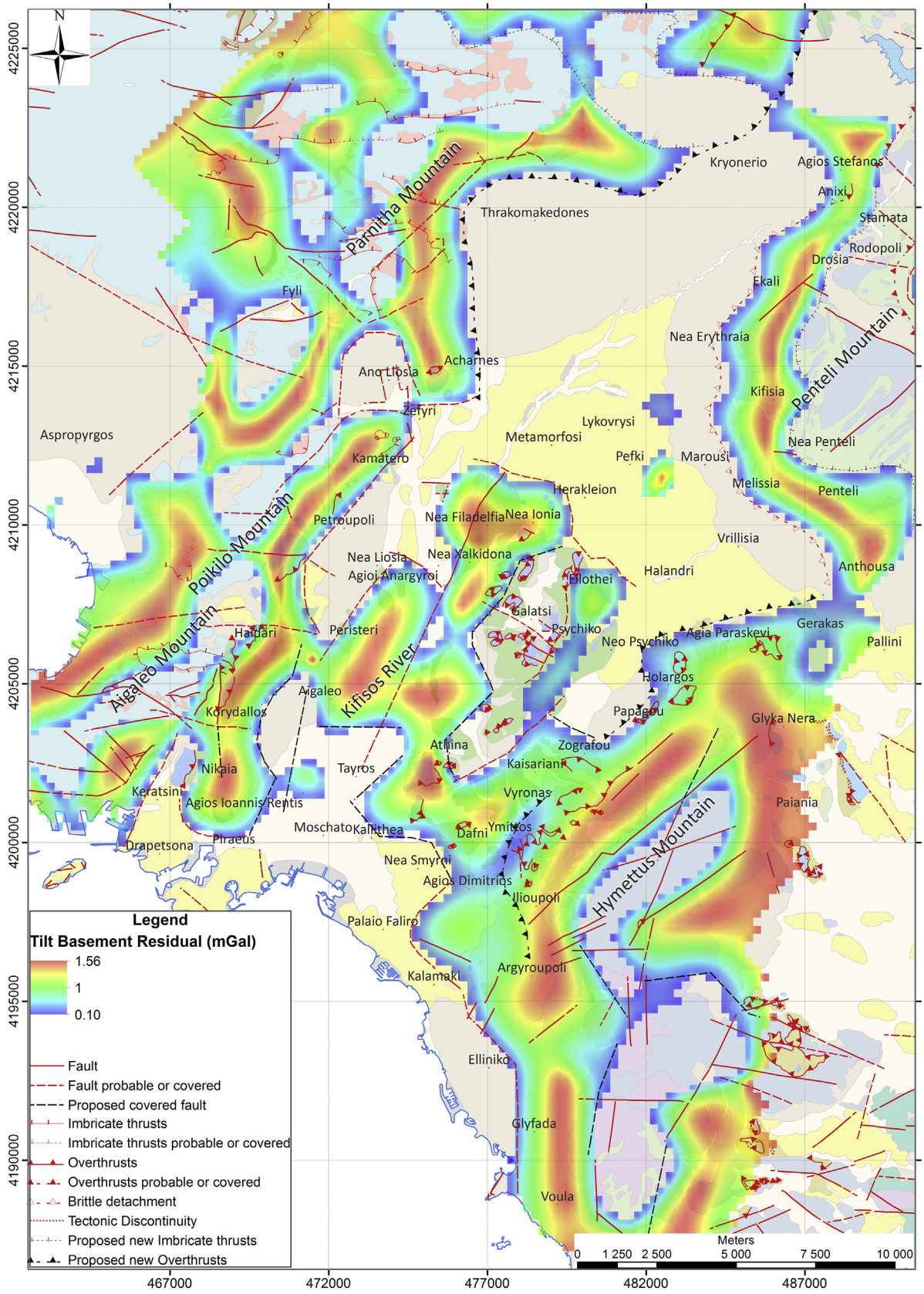

Fig. 16. Tilt derivative of residual data (deep structures).

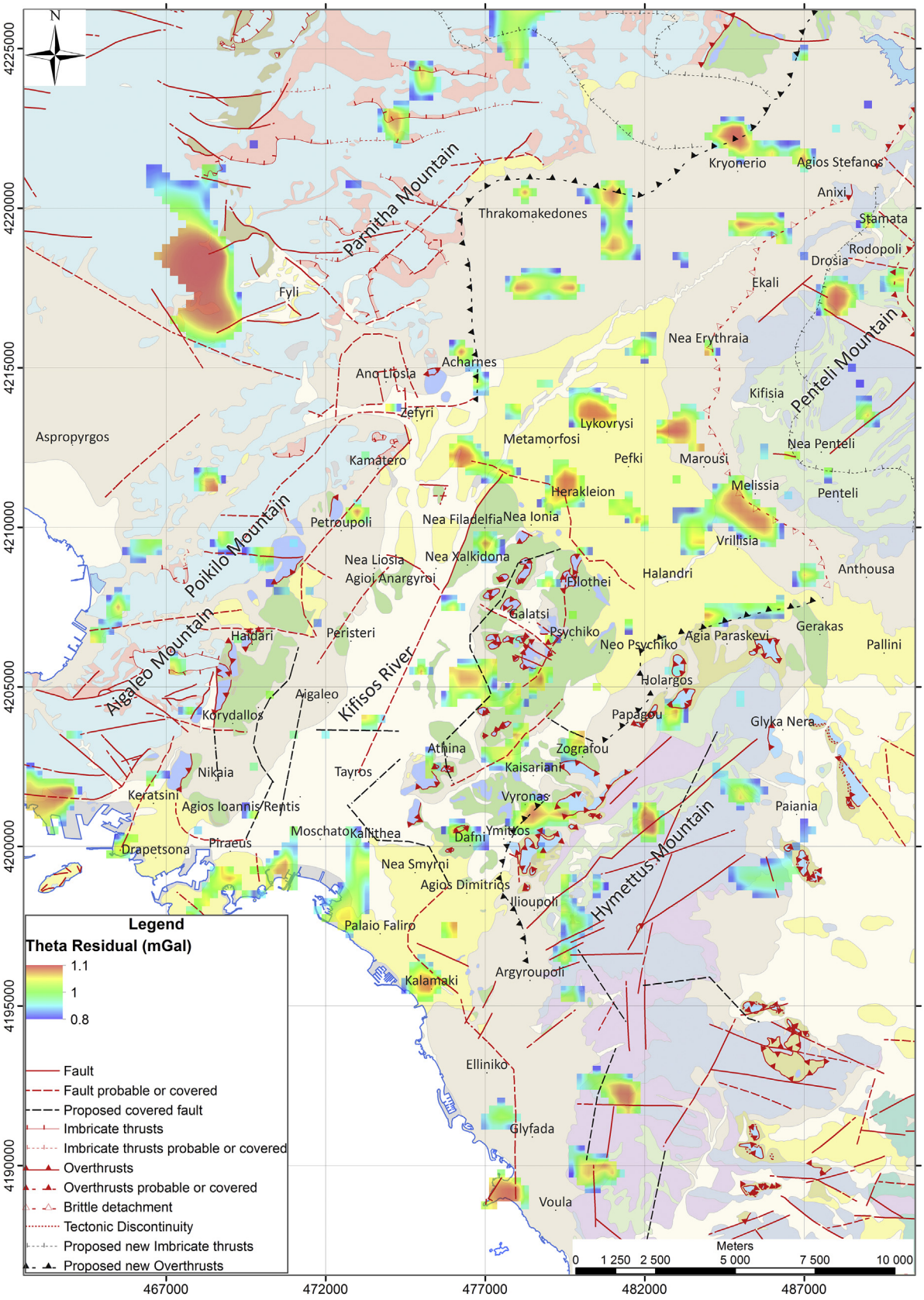

Fig. 17. Theta derivative of residual data (shallow structures).

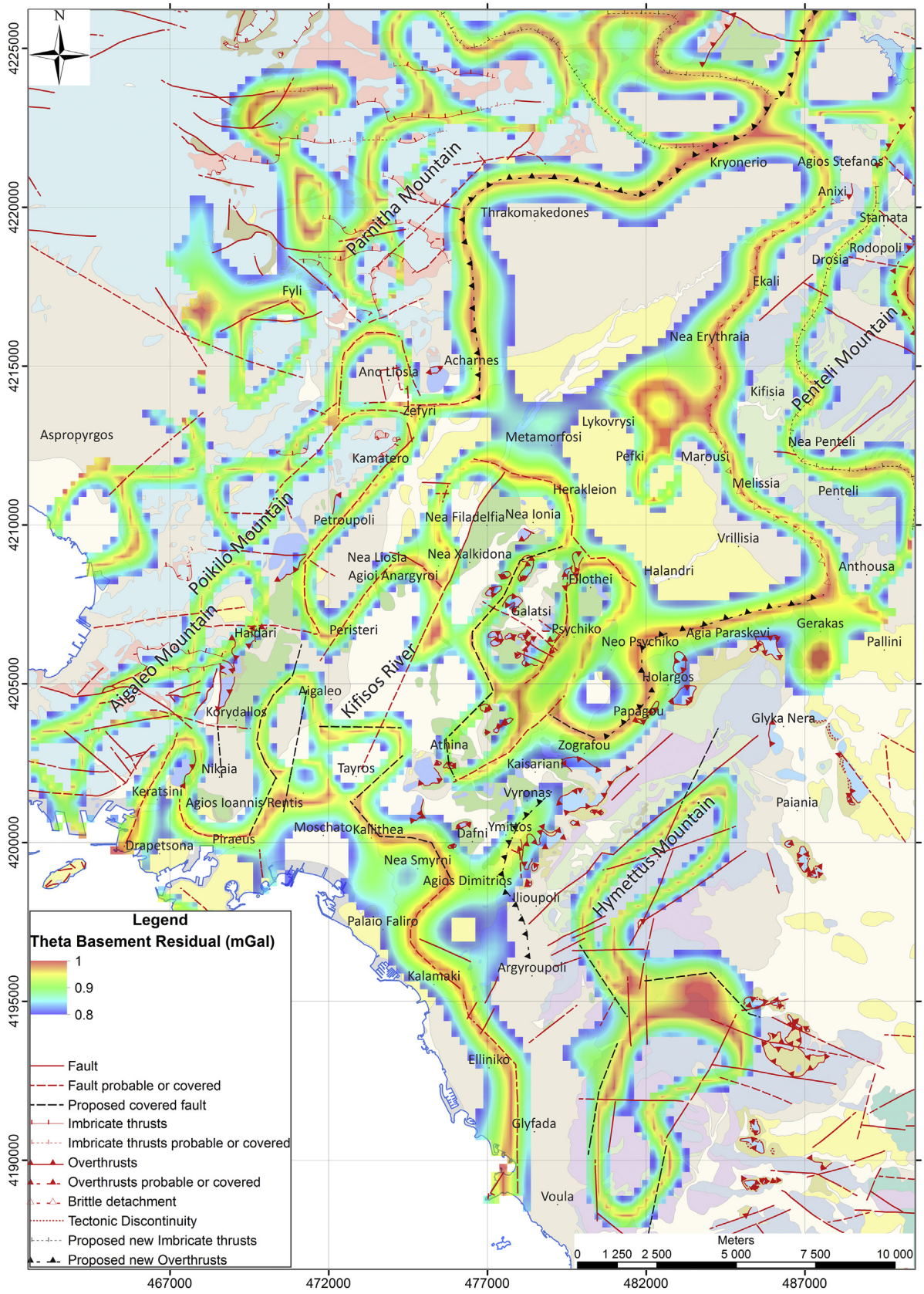

Fig. 18. Theta derivative of residual data (deep structures).

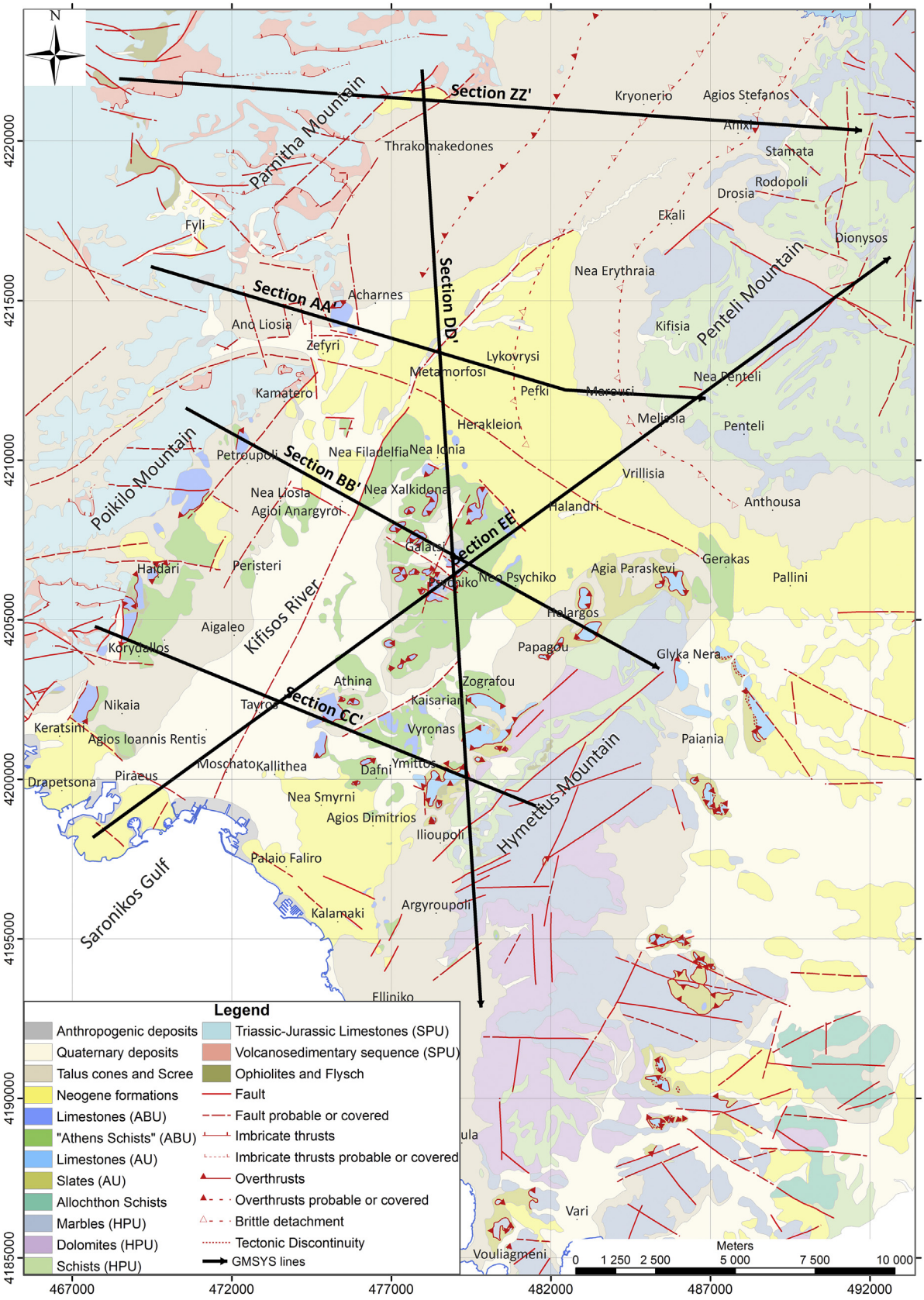

Fig. 19. The location of the profiles along the Athens basin, selected to create the interpretative geological-density 2.75-D models.

underlying *Alepovouni* Unit seems to justify the outcomes of the shallow structural maps, while the overthrust of the *Alepovouni Unit* above the *Athens* one produces the corresponding, more extended, results in the structural maps of the basement structures.

4.5. Interpretative 2.75D geological modelling

In the context of this paper, we have constructed 2.75D models of our gravity data, carried by GM-SYS, a program by *Geosoft*. It has been widely used the last few years (Ádám and Bielik, 1998; Ammirati et al., 2018; Azab and El-Khadragy, 2013; Blecha et al., 2009; Blaikie et al., 2014; Kim et al., 2009; Leader et al., 2006; Mancinelli et al., 2015; Park et al., 2006; Smith et al., 2006; Šumanovac et al., 2009; Weidmann et al., 2016). The 2.75D models can have 2D prisms asymmetrically positioned and extended at some distance from the line of the profile, in the strike direction. The model strike may also be tilted relative to the profile azimuth. Beyond the ends of these prisms, there are new ones of the same cross-section, but with different densities. It also allows independent specification of the locations of the two ends of the blocks (Geosoft, 2009).

In Fig. 19, the location of the profiles across the Athens basin, selected to create the interpretative geological-density 2.75-D models, is presented. A total of four (4) sections of total length equal to 87.5 km in several directions have been chosen, trying to adumbrate the tectonic framework of the area in all directions. The density values assigned to each block/prism are based on the adopted values (Table 3).

The known information from all the previous geological studies (described thoroughly in §2) along with personal observations have been taken into consideration in order to create models that present logical geological structures. Unfortunately, deep reliable borehole data have not been found in order to constrain the results. But, seismic profiles (Papadopoulos et al., 2007) have been recovered and compared with the gravity modelling in an effort to provide additional constraints for the final interpretative models.

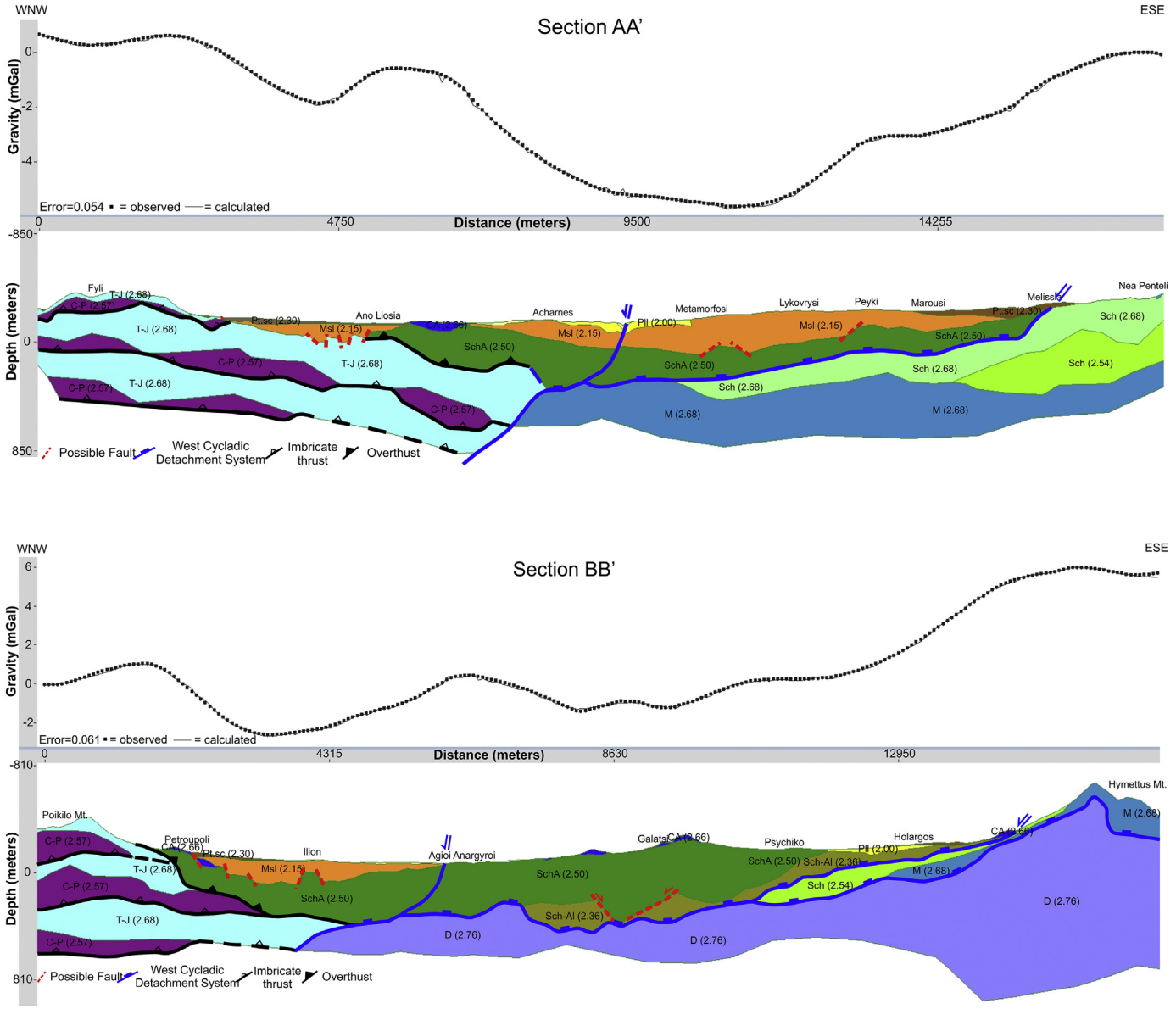

Fig. 20. Interpretative geological 2.75-D profiles, constructed with GM-SYS (scale 1:2). The observed (squares) and calculated (line) residual anomaly are illustrated. The geological formations are the following: T-J: Triassic-Jurassic limestones (*Sub-Pelagonian Unit*), C-P: Volcanosedimentary sequence (*Sub-Pelagonian Unit*), M: Marbles (*Hymettus-Penteli Unit*), Sch: Schists (*Hymettus-Penteli Unit*), D: Dolomites (*Hymettus-Penteli Unit*), SchA: Athens Schists (*Athens Basin Unit*), CA: Limestones (*Athens Basin Unit*), Sch—Al: Slates (*Alepovouni Unit*), Msl: Upper Miocene Terrestrial and Lacustrine deposits (*Neogene Formations*), Pll: Pliocene Terrestrial deposits (*Neogene Formations*), Pt.sc: Pleistocene talus and screes, Al: Alluvium deposits (*Loose Quaternary deposits*).

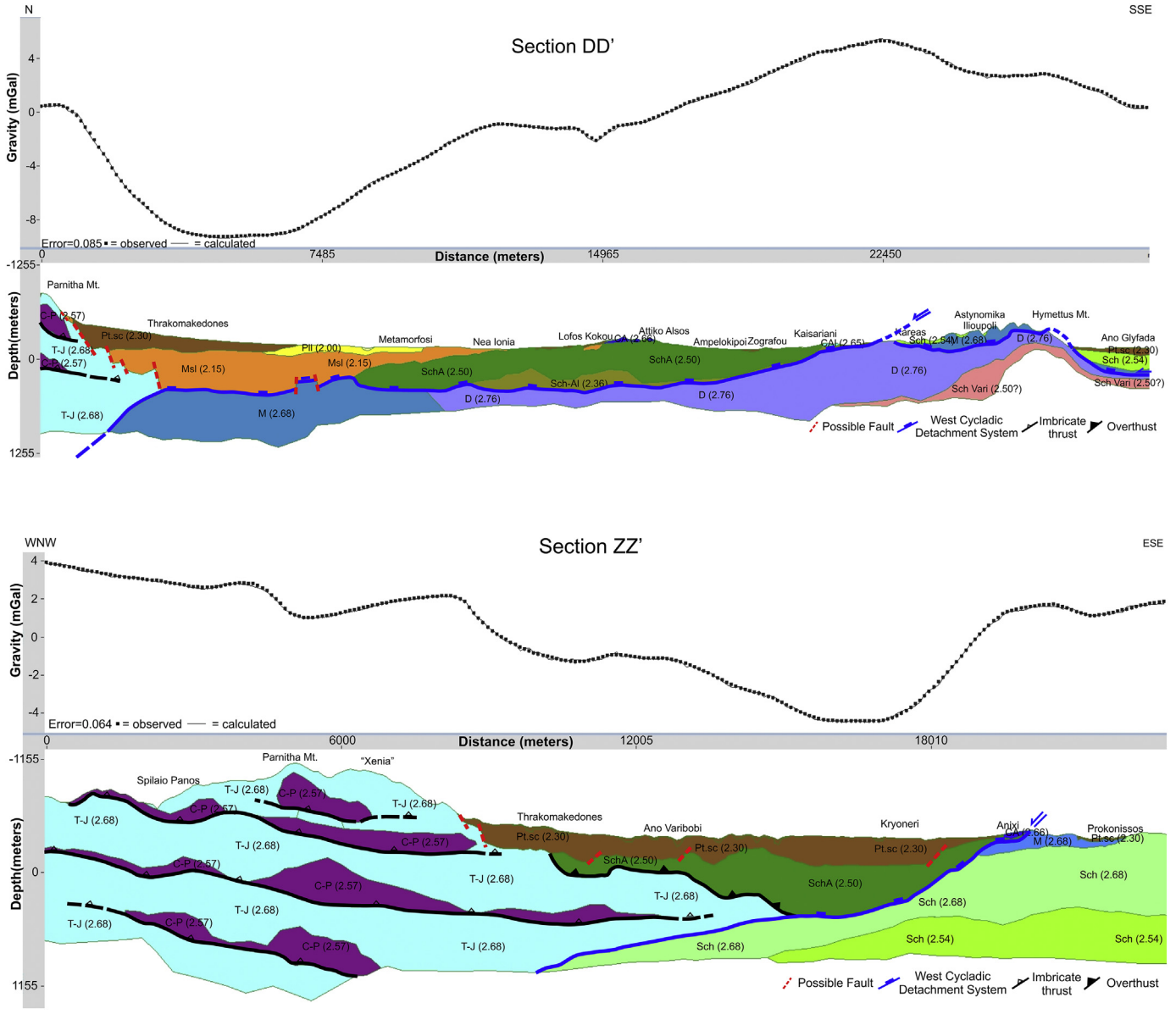

Fig. 21. Interpretative geological 2.75-D profiles, constructed with GM-SYS (scale 1:2). The observed (squares) and calculated (line) residual anomaly are illustrated. The geological formations are the following: T-J: Triassic-Jurassic limestones (*Sub-Pelagonian Unit*), C-P: Volcanosedimentary sequence (*Sub-Pelagonian Unit*), M: Marbles (*Hymettus-Penteli Unit*), Sch: Schists (*Hymettus-Penteli Unit*), D: Dolomites (*Hymettus-Penteli Unit*), SchA: Athens Schists (*Athens Basin Unit*), CA: Limestones (*Athens Basin Unit*), Sch—Al: Slates (*Alepovouni Unit*), Msl: Upper Miocene Terrestrial and Lacustrine deposits (*Neogene Formations*), Pll: Pliocene Terrestrial deposits (*Neogene Formations*), Pt.sc: Pleistocene talus and screes, Al: Alluvium deposits (*Loose Quaternary deposits*).

The careful and thorough determination of all the involved geological formations of Athens basin (Table 3), provide the first constrain during the production of our interpretative models (Figs. 20–21). Practically the other constraints used for these models are mostly geological, derived from the published literature that has already been discussed thoroughly in §2. The first information used as constrain comes from the updated surface geological map provided in Fig. 1. Afterwards, we have the relative positions, movements and tectonism of the four distinguished units and formations of our study area (discussed in detail in §2). We will shortly and simply remind that the geotectonic regime of the basin is constituted by the lower and relative autochthonous "*Hymettus-Penteli Unit*" (*HPU*), the overlying "*Sub-Pelagonian Unit*" (*SPU*) located along the western part of Athens basin, the "*Alepovouni Unit*" (*AU*) overlying at the eastern part of the basin and finally the upper tectonic unit "*Athens Basin Unit*" (*ABU*). Beyond that, the structural characteristics of the tectonic zones that control their relative placement in the basin, had been a controlling factor for the models. We are referring to major zones such as the detachment fault, which is considered to be part of the Western Cycladic Detachment System (*WCDS*) and other known significant thrusts. Among these major tectonic zones, we had also some constraints (dips, strikes etc.) regarding other mapped fault zones. Finally, for most of our interpretative models we had starting geological models (Papanikolaou et al., 2002).

The results of the interpretative geological-gravity 2.75-D sections are illustrated in Figs. 20–21. In each of these figures, the upper part illustrates the observed residual gravity data (squares) along with the calculated one (line) based on the geological model, which is illustrated on the lower part of the figures. Each block, colored differently simulates a geological body, with a certain density quoted in the brackets. The sections are presented with a vertical exaggeration of 2 for better presentation and understanding.

Along all the illustrated sections (Figs. 20–21), some common major fault zones have been delineated, revealing their systematic existence at the Athens subsurface. The detachment fault, as described by other authors (Coleman et al., 2018; Grasemann et al., 2012; Iglseder et al., 2011; Lekkas et al., 2011; Seman et al., 2012, 2013), seems to have been identified. Based on them, the underlying metamorphosed *Hymettus-Penteli Unit* is moving upwards relatively to the overlying tectonic units unmetamorphosed or weakly ones (based on the geological data). The slates and phyllites of *Athens Basin Unit* (Athens Schists, *SchA*) or the phyllites of *Alepovouni Unit* (*Sch—Al*) are mostly located above the detachment. On the other hand, the lithologies of the *Hymettus-Penteli Unit*, such as dolomites (*D*), schists (*Sch*) or even marbles (*M*) are below the detachment zone. Furthermore, at the first part of the sections three or four imbricate thrusts between the Triassic-Jurassic limestones (*T-J*) and the volcanosedimentary sequence (*C—P*), as defined by previous geological models (Papanikolaou, 2015; Papanikolaou et al., 2002, 2004b), seem to have been identified with different thickness. Beyond that, along most of the sections (AA', BB' and ZZ') we may also observe the existence of a thrust fault where the Athens Schists (*SchA*) of the *Athens Basin Unit* overlay tectonically the *Sub-Pelagonian Unit* described in older publications (Coleman et al., 2018; Krohe et al., 2010; Lekkas et al., 2011; Papanikolaou et al., 2002).

In Section AA' (Fig. 20), the Neogene formations (*Msl* and *Pll*) are observed with thickness up to 300 m below the areas of *Ano Liossia*, *Acharnes* and *Lykovrysi*, producing the low values in the residual gravity field (down to −5.8 mGal). Several neotectonic fault zones might have been revealed, mostly along the Neogene formations and their underlying alpine rocks, especially at the areas of *Ano Liossia*, *Metamorfosi* and *Lykovrysi*. Beneath the Neogene formations, the Athens Schists (*SchA*) are detected in the central part of the profile, with thickness up to 380 m. Below the *Penteli Mountain*, it seems that the schists (*Sch*) of the *Hymettus-Penteli Unit* are dominating over the marbles (*M*) that are detected mostly at its western foothills. Moreover, no dolomites (*D*) seem to be present.

In SectionBB' (Fig. 20), the Neogene formations (*Msl* and *Pll*) are observed with relatively smaller thickness (up to 170 m) and lateral coverage, below the areas of *Petroupoli*, *Agioi Anargyroi* and *Halandri*, producing the low values in the residual gravity field (down to −2.5 mGal). Several neotectonic fault zones might have been revealed, mostly along the Neogene formations and the underlying Athens Schists, between the areas of *Petroupoli* and *Ilion*. The Athens Schists (*SchA*) and the slates of *Alepovouni Unit* (*Sch—Al*) cover a great part of the subsurface underlying the Neogene formations, reaching a maximum thickness up to 500 and 225 m correspondingly. In this profile, the dolomites (*D*) of the *Hymettus-Penteli Unit* seem to dominate at the lower area below the basin (from a depth of 300 m) and the *Hymettus* Mountain, with thickness up to 1300 m. The slightly folded contact (detachment fault) between the Dolomites and the Upper Plate units (Figs. 20-21), which interprets the results of the geophysical, demonstrates the presence of constructional extension-parallel folds, a structure that is often observed in metamorphic core complexes and has also been observed in Athens basin (Lekkas and Lozios, 2000; Lozios, 1993).

In Section DD' (Fig. 21), the Neogene formations (*Msl* and *Pll*) are observed with great thickness, up to 580 and 130 m correspondingly, below the areas of *Thrakomakedones*, *Acharnes* and *Metamorfosi*, producing the low values in the residual gravity field (down to −8.5 mGal). They are placed directly on the detachment fault and with the other characteristics of the Late Miocene – Early Pliocene basin formations, they demonstrate being members of a supra-detachment basin, which is developed during the activation of the detachment fault as discussed in (Diamantopoulos et al., 2009; Friedrnann and Burbank, 1995; Krohe et al., 2010). A layer of almost 310 m of Pleistocene Talus and Screes (*Pt.sc*) is partially overlying the *Msl* deposits. More particularly, below the area of *Thrakomakedones*, several neotectonic fault zones have been revealed, between the post-alpine deposits and the underlying formations of *Sub-Pelagonian Unit*. The Athens Schists (*SchA*) and the slates of *Alepovouni Unit* (*Sch—Al*) cover a great part of the subsurface, underlying the Neogene formations, with great surface outcrops reaching a maximum thickness up to 530 and 270 m correspondingly. The marbles (*M*) and schists (*Sch*) of the *Hymettus-Penteli Unit* are also detected below the greater area of *Hymettus Mountain* as well as below the area of *Thrakomakedones*. The dolomites (*D*) of the *Hymettus-Penteli Unit* seem to dominate at the central area of the section, below the basin (from depths of 600 m) and below the *Hymettus* Mt., with thickness that reaches 750 m. Beneath them, the formation of Vari Schists (*Sch Vari*) is also expected.

In Section ZZ' (Fig. 21), a thick layer of Pleistocene Talus and Screes (*Pt.sc*) is observed at the central area of the section, below *Thrakomakedones*, *Kryoneri* and *Agios Stefanos* areas, with thickness up to 290 m, producing the low values in the residual gravity field (down to −4.5 mGal). Especially, below the area of *Thrakomakedones*, several neotectonic fault zones have been revealed, between the Pleistocene Talus and Screes (*Pt.sc*) and the underlying formations of *Sub-Pelagonian Unit*. The Athens Schists (*SchA*) cover a great part of the subsurface, beneath the Pleistocene talus and screes (*Pt.sc*), with thickness up to 540 m. Below *Penteli Mountain*, it seems that the schists (Sch) are dominating over the marbles (*M*), with thicknesses that reach 1350 m and 175 m correspondingly. On the contrary, the dolomites (*D*) of the *Hymettus-Penteli Unit* have not been identified.

5. Discussion

The dominant tectonic structure of Athens basin is represented by a major detachment zone, part of the West Cycladic Detachment System (Coleman et al., 2018; Grasemann et al., 2012; Iglseder et al., 2011; Lekkas et al., 2011; Seman et al., 2012, 2013), which is responsible for the exhumation of the foot-wall block metamorphic rocks. This low-angle fault zone has been identified in most of the models (Figs. 20–22), where un- or weakly metamorphosed rocks appear on the hanging wall block. Through some of the interpretative profiles, mainly those of WNW-ESE orientation, both the fault surface and the schistosity of the exhumed metamorphic rocks, seem to have a curviplanar geometry, especially below the Hymettus Mt. (Figs. 20–22). These dome shaped structures are elongated along the stretching direction, which is indicated by the N-S oriented stretching lineation associated with the detachment zone, and therefore they can be interpreted as extension-parallel folds, formed in a constrictive extensional regime (Avigad et al., 2001; Levy and Jaupart, 2011; Le Pourhiet et al., 2012). This metamorphic core-complex structure is completed by a supra-detachment basin (Diamantopoulos et al., 2009; Friedrnann and Burbank, 1995; Krohe et al., 2010) and is filled with Late Miocene – Early Pliocene sediments (Figs. 20–22), as the tectono-sedimentary characteristics of Athens basin (fault geometry, drainage direction, depocenter, sediment character etc.) reveal (Papanikolaou et al., 2002, 2004a). The produced models suggest that the thickness of the basin sediments ranges around 800–900 m.

At the eastern margin of Athens basin, the extent of a major thrust has also been detected, since as shown by the interpretative profiles, the phyllites of Athens Schists (*SchA*), are overlying the Triassic-Jurassic limestones (*T-J*) of the (unmetamorphosed) Sub-Pelagonian Unit. Beyond these, the existence of 3–4 successive imbricate thrusts, between different lithologies of the Sub-Pelagonian Unit, seems to have been adumbrated, based on the interpretation of the gravity results.

A major tectonic line along the main route of *Kifisos River* (Fig. 1) has been suggested by several researchers (Fountoulis, 2004; Lekkas, 2001; Mariolakos and Fountoulis, 2000; Papanikolaou et al., 2002, 2004a, 2004b) and seems to be related with the tectonic boundary between the *Hymettus-Penteli* metamorphosed Unit and the Sub-Pelagonian non-metamorphosed Unit. It is represented by an NNE-SSW (dipping to the WNW) listric normal fault, which roots into the detachment zone. It has a steep geometry at its upper part, near the surface, and

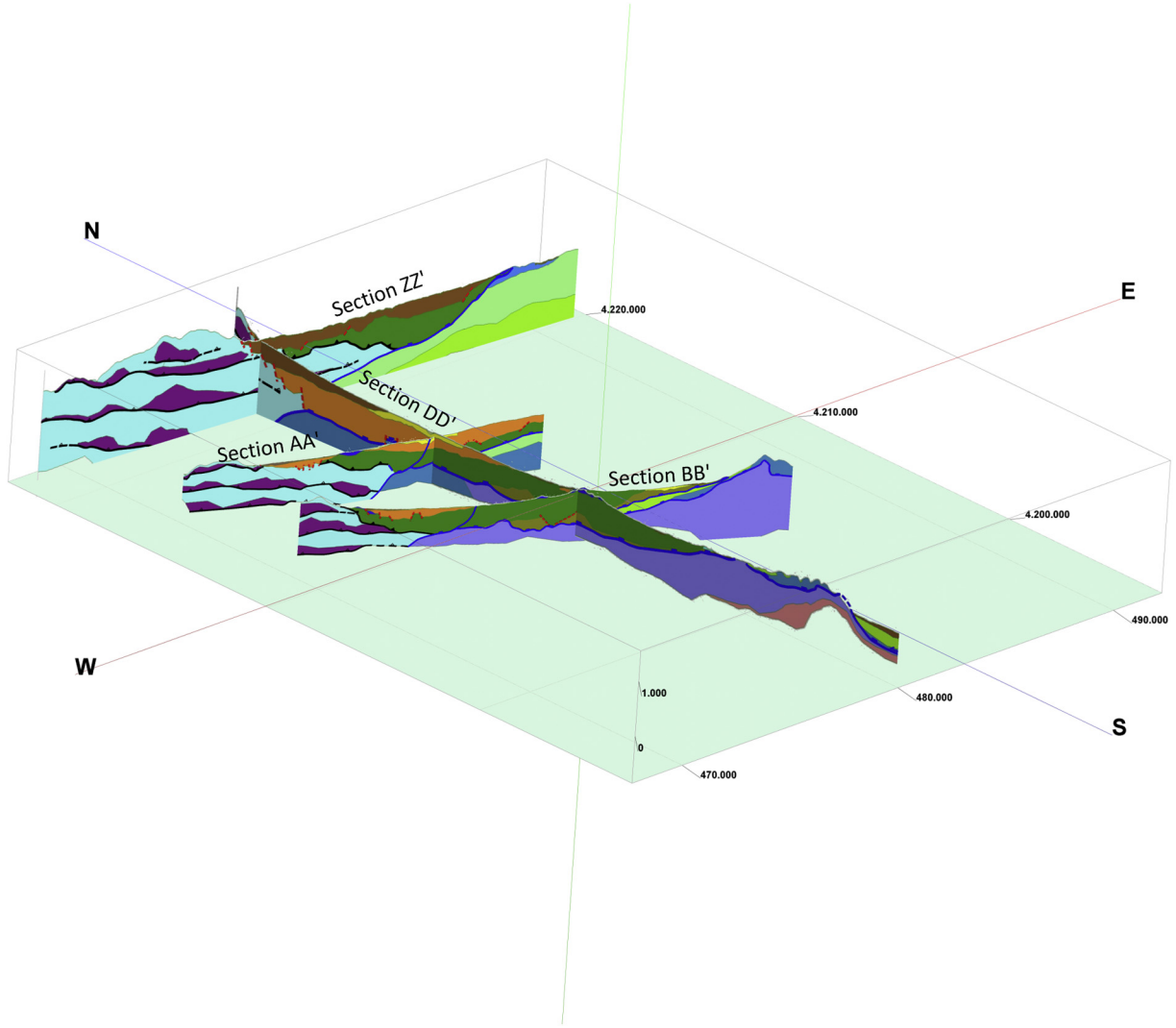

Fig. 22. 3D illustration of the interpretative geological profiles (looking from SW and scale 1:2).

becomes low-angle where it roots into the detachment. This fault played a significant role in the damage distribution of September 9th, 1999 destructive earthquake (Ms = 5,9R), the damage is both bounded and directed along the hanging wall (the western half of the basin), based on (Lekkas, 2001; Tzitziras et al., 2000).

A first approach is illustrated in the structural maps of Figs. 9–18. We could say that in general, this major tectonic zone does exist, but its trace needs to be redefined [1]. The southern part seems to have been identified by the gravity results but restricted in length, between *Tavros* and *Metamorfosi* (Fig. 23). Regarding its northern part and more specifically between *Thrakomakedones* and *Acharnes*, it has been relocated a few kilometers westernmost, following the southern foothills of *Parnitha* Mountain, with a trace similar to an approach of Krohe et al., 2010

Another significant WNW-ESE probable fault zone which seems to be related with the damage distribution of February–March 1981 destructive earthquake sequence (Ms 6,7; 6,4; 6,3), is also suggested by the same researchers (Papanikolaou et al., 2002, 2004a, 2004b). According to Krohe et al. (2010), a part of this zone probably identified with the brake-away fault of the detachment zone. The fault zone, which extends from *Zefyri* to *Agia Paraskevi* [2], has also been partially confirmed by the structural maps (Figs. 9–18), mainly in the area between *Halandri* and *Kokkinos Mylos* areas (Fig. 23) but slightly relocated to the southern. On the other hand, its western extension, along the western foothills of *Aigaleo-Poikilo* Mountains, has not been verified for all its length and has also been relocated a couple kilometers easternmost.

Moreover, two significant probable NNE-SSW fault zones seem to have also been identified undoubtedly in the western suburbs of the basin. These fault zones are along *Kamatero-Petroupoli* [3] and *Agioi Anargyroi-Peristeri* [4], in Fig. 23, with estimated throws of at least 80 m. The first one could be extended to southern-easternmost. At the north-west expanse of the basin, a few smaller N-S covered faults, at the areas of *Ano Liosia*, *Zefyri* and *Acharnes* [5] are also adumbrated in the gravity maps with estimated throws ranging between 40 and 90 m. Furthermore, close to westward of *Thrakomakedones*, at the southern foothills of *Parnitha* Mountain [6], a NE-SW fault, mapped as probable, seems to have been verified with throws up to 220–250 m.

At the south-west part of Athens basin (Fig. 23), several other fault zones have been identified. One W-E is located in *Haidari* [7], one NNE-SSW at *Keratsini* but extended southern to *Drapetsona* [8] based on the new data and the other one W-E along *Keratsini-Piraeus* [9], with estimated throw of 150 m. Additionally, the almost W-E fault of *Korydallos* [10] not only has been verified but can also be elongated up to *Nikaia*. Looking at the central region of Athens basin (Fig. 23), the fault zone of *Filothei-Galatsi-Gkyzi* [11], with direction almost N-S, has been relocated slightly to the east. The probable fault zones along

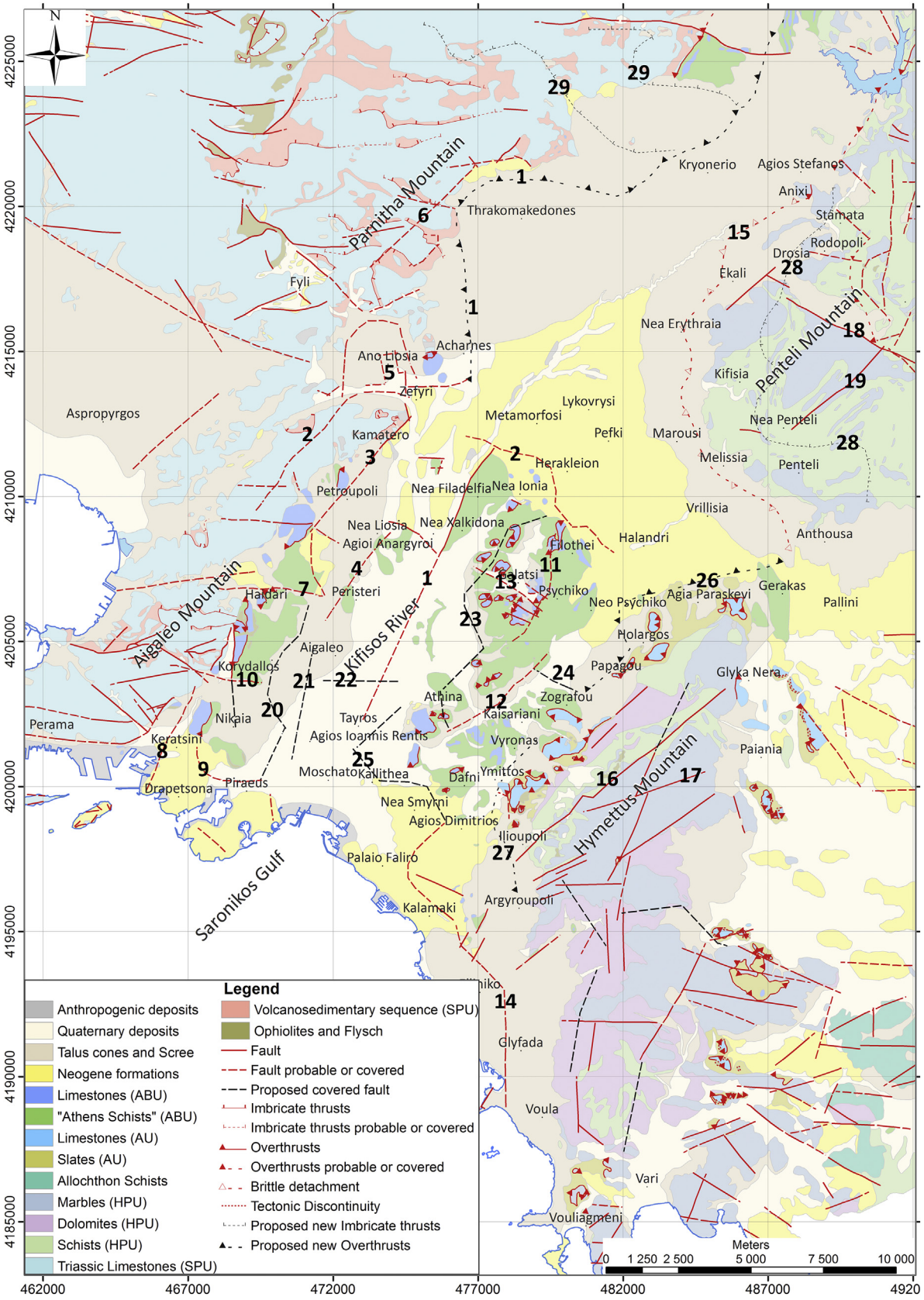

Fig. 23. Updated geological and tectonic map, based on the results of the gravity survey. The modification of older probable concealed faults and the proposal of new ones are illustrated with black dashed lines.

Zografou-Fix [12] with direction NE-SW and the NW-SE *Galatsi-Psychiko* [13] provided indications in the gravity data that increase the possibility of their existence.

Furthermore, at the southern suburbs (Fig. 23), the zone of *Kalamaki* [14] has also been identified, but beyond that, we have severe indications based on the gravity results for a great extension towards the areas of *Elliniko-Glyfada-Voula*, along which the direction shifts from NW-SE to almost N-S. Northernmost, along the western and southern foothills of *Penteli* Mountain (Fig. 23), the probable overthrust of Upper Cretaceous [15] has been delineated undoubtedly by the gravity measurements almost at the location that was expected to be (*Anixi-Ekali-Nea Erythraia-Marousi-Melissia-Anthousa*), with direction from NE-SW, shifted to N-S and then to NW-SE.

The fact that several major visible faults zones have also been verified on the mountains of *Hymettus*, *Penteli* and *Parnitha* (Fig. 23) increases the credibility of our results. Some examples of them are running NE-SW along the areas *Glyka Nera-Ilioupoli* [16], *Paiania-Ilioupoli* [17], *Rapendosa-Nea Penteli* [19] and NW-SE along *Rea-Dionysos* [18].

Apart from the confirmation of already delineated fault zones, either as visible or probably covered, we have indications based on the gravity measurements that allow us to propose additional locations of probable faults. Beginning from the western suburbs, three new fault zones may have been detected (Fig. 23) NNE-SSW along the areas of Ag*ia Varvara-Korydallos-Agios Ioannis Rentis-Piraeus* [20], *Aigaleo-Agios Ioannis Rentis* [21] and W-E along *Aigaleo-Votanikos* [22].

Additionally, at the central expanse of the area, more probable fault zones may have been delineated along the areas of *Nea Ionia-Galatsi-Kypseli-Downtown-Fix* [23] continuously altering its direction between NNE-SSW and NNE-SSE and a smaller one *Ampelokipoi-Zografou* [24] with WBW-ESE direction (Fig. 23). A few kilometers southern, a new system of fault zones has been revealed, running along *Petralona-Kallithea-Nea Smyrni-Agios Dimitrios-Palaio Faliro* [25], with altering directions (NE-SW, NW-SE and W-E). This system could be merged with the one that we have already mentioned, across the areas of *Palaio Faliro-Kalamaki-Elliniko-Glyfada-Voula* [14].

Along the eastern part of the basin, the gravity results delineate a major tectonic discontinuity along the western foothills of mountain *Hymettus* and more specifically along the areas *Gerakas-AgiaParaskevi-NeoPsychiko-Holargos-Papagou-Zografou* [26], with varying directions (ENE-WSW, NNE-SSW and NE-SW) and then again along *Vyronas-Ilioupoli-Argyroupoli* [27] with directions NE-SW and then NW-SE (Fig. 23). This zone seems to match with an extended brittle low-angle normal fault that separates the overlying Athens Basin Unit from the underlying Alepovouni Unit.

At the northern suburbs, we can adumbrate a few new fault zones, located on the mountains *Penteli* and *Parnitha* (Fig. 23). More specifically, we have a major brittle detachment along *Stamata-Rodopoli-Drosia-Kifisia-Nea Penteli* [28], with direction from NE-SW, shifted to N-S and then to NW-SE. Additionally, two or three major imbricate thrusts could be indicated west of *Kryoneri* and *Drosopigi* [29], with directions close to NW-SE and W-E. Beyond these, on the surrounding mountains of Athens basin, there are several other locations indicating the possible existence of smaller fault zones, based on the gravity results.

6. Conclusions

The application of three different methods for the determination of the densities of the geological formations has been more than helpful. Because of that, we were able to define the density of all the formations, even of the ones compiled of different lithologies, such as the Neogene formations and the Athens Schists. The application of Nettleton method for determining the density of the Neogene formations and Quaternary sediments, because they were either too unconsolidated to be measured in the laboratory or they were comprised of several different lithologies. Each lithology has its own density that was calculated through laboratory measurements but the final representative value of the whole formation could not be estimated. The density profiles were equally helpful in the case of the Athens Basin Unit (*ABU*), which are considered to be a mélange. On the other hand, the densities for the most alpine formations were based on accurate laboratory measurements. Finally, for the cases of the loose alluvial deposits (*Q-Al*) and the inhomogeneous talus cones & scree (*Pt. sc*), the conversion of the seismic velocity data provided the necessary information.

The qualitative structural maps seem to contribute a lot to the identification of the fault zones providing impressive images. This means that we can both identify and propose new locations of blind faults or we can verify and modify the location of already proposed as covered faults zones from other studies.

We managed to interpret the results by constructing the 2.75D geological models, based on the gravity response of the collected data. Based on Figs. 20–22 and their analysis, important data regarding the thickness of the geological formations covering the basin were recovered.

Therefore, based only on the constructed interpretation models (Figs. 20–22) the geological formations are observed with corresponding maximum thickness:

- Alluvium deposits (*Al*) up to of 40–50 m.
- Pleistocene Talus and Screes (*Pt.sc*) up to 310 m, below *Thrakomakedones*, *Kryoneri* and *Agios Stefanos* areas.
- Neogene formations (*Msl* and *Pll*) up to a total of 550 m, below the areas of *Thrakomakedones*, *Acharnes*, *Lykovrysi* and *Metamorfosi*.
- The formation of Athens Schists (*SchA*), representing the lower part of Athens Basin Unit (*ABU*), covering great extent of the Athens basin, up to 600 m.
- The slates of Alepovouni Unit (*Sch—Al*), up to 270 m.
- The dolomites (*D*) of Hymettus-Penteli Unit (*HPU*), up to 1300 m.
- The Schists (*Sch*) of Hymettus-Penteli Unit (*HPU*), close to 1750 m.

Based on the models, illustrated in Figs. 20–22, we can interpret the subsurface structure of Athens basin for depths up to 2500 m. The authors took into consideration all the published studies regarding the structural regime of Athens basin (mentioned in the previous paragraphs) and tried to reveal some of them through the models. Some of the interpreted zones are: i)old thrust faults and imbricate thrusts, ii) a major (low-angle) detachment zone, considered to be part of the *West Cycladic Detachment System*, responsible for the exhumation of Attica metamorphic rocks, iii) extension-parallel folds that deform both the detachment and the schistosity, iv) a supra-detachment basin, filled with Late Miocene – Early Pliocene sediments and v) younger high-angle neotectonic faults, that root into the detachment.

The interpretation of the collected data proved to be valuable as we have obtained important new information about the majority of the geological and tectonic structures of Athens basin, but we have also tried to delineate the subsurface structure in order to identify new concealed urban fault zones. These zones are very important because some of them may have the potential to generate disastrous earthquakes that will result in heavy casualties and significant economic loss, especially if we take into consideration the importance of Athens metropolis. It is also important that even the fault zones which are no longer active seem to play a significant role in damage distribution, as they can direct, block or enhance the seismic energy.

Acknowledgments

The fieldwork was supported by the Special Account for Research Grants of the UoA (contract no. 70/4/9254). The authors would like to thank Ms. Achtypi S., Ms. Kaplanidi H., Mr. Papaelias S., Mr. Mavroulis

S., Mr. Michelioudakis D.and Ms. Drosopoulou E. for their valuable contribution to the field measurements. The authors would also like to thank Ms. Mitsika Georgia for her contribution during the construction of the 3D illustrations. Finally, the authors would like to thank Assist. Professor Dr. Aikaterini Kouli, for her permission to have access and use laboratory equipment, useful for the density determination.

References

Abzalov, M.Z., 2013. Measuring and modelling of dry bulk rock density for mineral resource estimation. Appl. Earth Sci. 122 (1), 16–29. https://doi.org/10.1179/1743275813Y.0000000027.

Ádám, A., Bielik, M., 1998. The crustal and upper-mantle geophysical signature of narrow continental rifts in the Pannonian basin. Geophys. J. Int. 134 (1), 157–171. https://doi.org/10.1046/j.1365-246x.1998.00544.x.

Al-Banna, A.S., Al-Karadaghi, S.S., 2018. Integration study of a new gravity and seismic survey along NE-SW profile in Al-Najaf Desert. Iraqi J. Sci. 59 (1B), 314–328. https://doi.org/10.24996/ijs.2018.59.1B.10.

Alexopoulos, J.D., Fountoulis, I., Kambouris, P., Mariolakos, I., Papadopoulos, T.D., 2001. Geoelectrical survey for Tatoi (Athens, Greece) blind fault. Bull. Geol. Soc. Greece 24 (1), 121–127 (*In Greek*). 10.12681/bgsg.16951.

Ali, H.O., Whiteley, R.J., 1981. Gravity exploration for groundwater in the Bara Basin, Sudan. Geoexploration 19 (2), 127–141. https://doi.org/10.1016/0016-7142(81)90025-9.

Ali, M.Y., Fairhead, J.D., Green, C.M., Noufal, A., 2017. Basement structure of the United Arab Emirates derived from an analysis of regional gravity and aeromagnetic database. Tectonophysics 712-713, 503–522. https://doi.org/10.1016/j.tecto.2017.06.006.

Altherr, R., Kreuzer, H., Wendt, I., Lenz, H., Wagner, G.A., Keller, J., Harre, W., Hohndorf, A., 1982. A late Oligocene/early Miocene high temperature belt in the Attic-Cycladic crystalline Complex (S.E. Pelagonian, Greece). Geol. Jahrb. E23, 97–164.

Ammirati, J.B., Venerdini, A., Alcacer, J.M., Alvarado, P., Miranda, S., Gilbert, H., 2018. New insights on regional tectonics and basement composition beneath the eastern Sierras Pampeanas (Argentine back-arc region) from seismological and gravity data. Tectonophysics 740, 42–52. https://doi.org/10.1016/j.tecto.2018.05.015.

Anderson, M., Matti, J., Jachens, R., 2004. Structural model of the San Bernardino basin, California, from analysis of gravity, aeromagnetic, and seismicity data. J. Geophys. Res. Solid Earth 109 (B4). https://doi.org/10.1029/2003JB002544.

Antoniou, V., 2000. Geoenvironmental Conditions of Athens Basin Using Geographical Information Systems. PhD Thesis. Agricultural University of Athens (286p. In Greek). http://hdl.handle.net/10442/hedi/11977.

Anudu, G.K., Stephenson, R.A., Macdonald, D.I., Oakey, G.N., 2016. Geological features of the northeastern Canadian Arctic margin revealed from analysis of potential field data. Tectonophysics 691, 48–64. https://doi.org/10.1016/j.tecto.2016.03.025.

Apostolopoulos, G., Pavlopoulos, K., Goiran, J.P., Fouache, E., 2014. Was the Piraeus peninsula (Greece) a rocky island? Detection of pre-Holocene rocky relief with borehole data and resistivity tomography analysis. J. Archaeol. Sci. 42, 412–421. https://doi.org/10.1016/j.jas.2013.11.026.

Avigad, D., Ziv, A., Garfunkel, Z., 2001. Ductile and brittle shortening, extension-parallel folds and maintenance of crustal thickness in the Central Aegean (Cyclades, Greece). Tectonics 20 (2), 277–287. https://doi.org/10.1029/2000TC001190.

Azab, A.A., El-Khadragy, A.A., 2013. 2.5-D gravity/magnetic model studies in Sahl El Qaa Area, Southwestern Sinai, Egypt. Pure Appl. Geophys. 170 (12), 2207–2229. https://doi.org/10.1007/s00024-013-0650-5.

Baptiste, J., Martelet, G., Faure, M., Beccaletto, L., Reninger, P.A., Perrin, J., Chen, Y., 2016. Mapping of a buried basement combining aeromagnetic, gravity and petrophysical data: the substratum of southwest Paris Basin, France. Tectonophysics 683, 333–348. https://doi.org/10.1016/j.tecto.2016.05.049.

Berrocal, J., Marangoni, Y., de Sá, N.C., Fuck, R., Soares, J.E., Dantas, E., Perosi, F., Fernandes, C., 2004. Deep seismic refraction and gravity crustal model and tectonic deformation in Tocantins Province, Central Brazil. Tectonophysics 388 (1–4), 187–199. https://doi.org/10.1016/j.tecto.2004.04.033.

Blaikie, T.N., Ailleres, L., Betts, P.G., Cas, R.A.F., 2014. Interpreting subsurface volcanic structures using geologically constrained 3-D gravity inversions: examples of maar-diatremes, Newer Volcanics Province, southeastern Australia. J. Geophys. Res. Solid Earth 119 (4), 3857–3878. https://doi.org/10.1002/2013JB010751.

Blecha, V., Štemprok, M., Fischer, T., 2009. Geological interpretation of gravity profiles through the Karlovy Vary granite massif (Czech Republic). Stud. Geophys. Geod. 53 (3), 295–314. https://doi.org/10.1007/s11200-009-0019-5.

Boszczuk, P., Cheng, L.Z., Hammouche, H., Roy, P., Lacroix, S., Cheilletz, A., 2011. A 3D gravity data interpretation of the Matagami mining camp, Abitibi Subprovince, Superior Province, Québec, Canada: Application to VMS deposit exploration. J. Appl. Geophys. 75 (1), 77–86. https://doi.org/10.1016/j.jappgeo.2011.06.031.

Bouckovalas, G.D., Kouretzis, G.P., 2001. Stiff soil amplification effects in the 7 September 1999 Athens (Greece) earthquake. Soil Dyn. Earthq. Eng. 21 (8), 671–687. https://doi.org/10.1016/S0267-7261(01)00045-8.

Brocher, T.M., 2005. Empirical relations between elastic wavespeeds and density in the Earth's crust. Bull. Seismol. Soc. Am. 95 (6), 2081–2092. https://doi.org/10.1785/0120050077.

de Castro, D.L., Fuck, R.A., Phillips, J.D., Vidotti, R.M., Bezerra, F.H., Dantas, E.L., 2014. Crustal structure beneath the Paleozoic Parnaíba Basin revealed by airborne gravity and magnetic data, Brazil. Tectonophysics 614, 128–145. https://doi.org/10.1016/j.tecto.2013.12.009.

Chaubey, A.K., Rao, D.G., Srinivas, K., Ramprasad, T., Ramana, M.V., Subrahmanyam, V., 2002. Analyses of multichannel seismic reflection, gravity and magnetic data along a regional profile across the central-western continental margin of India. Mar. Geol. 182 (3–4), 303–323. https://doi.org/10.1016/S0025-3227(01)00241-9.

Coleman, M., Soukis, K., Schnider, D., Grasemann, B., Lozios, S., 2018. The northwest termination of the West Cy-cladic Detachment System in Central Attica. EGU General Assembly Conference Abstracts. vol. 20, p. 5172.

Cooper, G.R., Cowan, D.R., 2008. Edge enhancement of potential-field data using normalized statistics. Geophysics 73 (3), H1–H4. https://doi.org/10.1190/1.2837309.

Damaceno, J.G., de Castro, D.L., Valcácio, S.N., Souza, Z.S., 2017. Magnetic and gravity modeling of a Paleogene diabase plug in Northeast Brazil. J. Appl. Geophys. 136, 219–230. https://doi.org/10.1016/j.jappgeo.2016.11.006.

Diamantopoulos, A., Krohe, A., Mposkos, E., 2009. Kinematics of conjugate shear zones, displacement partitioning and fragmentation of the upper rigid crust during denudation of high-P rocks (Pelagonian and Sub-Pelagonian zones, Greece). Tectonophysics 473 (1–2), 84–98. https://doi.org/10.1016/j.tecto.2008.05.028.

Dilalos, S., 2018. Application of Geophysical Technique to the Investigation of Tectonic Structures in Urban and Suburban Environments. A Case Study in Athens Basin. Ph. D. Thesis. National and Kapodistrian University of Athens, Athens, Greece 321p.

Dilalos, S., Alexopoulos, J.D., 2017. Indications of correlation between gravity measurements and isoseismal maps. A case study of Athens basin (Greece). J. Appl. Geophys. 140, 62–74. https://doi.org/10.1016/j.jappgeo.2017.03.012.

Dilalos, S., Alexopoulos, J.D., Tsatsaris, A., 2018. Calculation of Building Correction for urban gravity surveys. A case study of Athens metropolis (Greece). J. Appl. Geophys. 159 (C), 540–552. https://doi.org/10.1016/j.jappgeo.2018.09.036.

Dürr, S., Altherr, R., Keller, J., Okrusch, M., Seidel, E., 1978. The Median Aegean Crystalline Belt: Stratigraphy, Structure, Metamorphism, Magmatism, *Alps*, *Apennines*, *Hellenides*. vol. 38 pp. 455–476.

Elkhodary, S.T., Youssef, M.A.S., 2013. Integrated potential field study on the subsurface structural characterization of the area North Bahariya Oasis, Western Desert, Egypt. Arab. J. Geosci. 6 (9), 3185–3200. https://doi.org/10.1007/s12517-012-0590-x.

Eshaghzadeh, A., 2015. Image edge detection of the total horizontal gradient of gravity data using the normalized tilt angle. Geodynam. Res. Int. Bull. 3 (4), 28–33.

Fairhead, J.D., 2015. Advances in Gravity and Magnetic Processing and Interpretation. EAGE Publications, The Netherlands (338p. ISBN 978-94-6282-175-0).

Fernandez-Cordoba, J., Zamora-Camacho, A., Espindola, J.M., 2017. Gravity Survey at the Ceboruco Volcano Area (Nayarit, Mexico): a 3-D Model of the Subsurface Structure. Pure Appl. Geophys. 174 (10), 3905–3918. https://doi.org/10.1007/s00024-017-1600-4.

Fountoulis, I., 2004. The neotectonic macrostructures and the geological basement, the main factors controlling the spatial distribution of the damage and geodynamic phenomena resulting from the Kalamata (13 September 1986) and Athens (7 September 1999) earthquakes. Earthquake Geodynamics: Advances in Earthquake Engineering, pp. 45–67.

Freyberg, B.V., 1951. Das Neogen-Gebiet nordwestlich Athen. Ann. Géol. Pays Hellén. 3, 65–86 (In German).

Friedrnann, S.J., Burbank, D.W., 1995. Rift basins and supradetachment basins: intracontinental extensional end-members. Basin Res. 7 (2), 109–127. https://doi.org/10.1111/j.1365-2117.1995.tb00099.x.

Gabtni, H., Jallouli, C., 2017. Regional-residual separation of potential field: an example from Tunisia. J. Appl. Geophys. 137, 8–24. https://doi.org/10.1016/j.jappgeo.2016.12.011.

García-Pérez, T., Marquardt, C., Yáñez, G., Cembrano, J., Gomila, R., Santibañez, I., Maringue, J., 2018. Insights on the structural control of a Neogene forearc basin in Northern Chile: a geophysical approach. Tectonophysics. 736, 1–14. https://doi.org/10.1016/j.tecto.2018.04.003.

Gardner, G.H.F., Gardner, L.W., Gregory, A.R., 1974. Formation velocity and density -the diagnostic basics for stratigraphic traps. Geophysics 39 (6), 770–780. https://doi.org/10.1190/1.1440465.

Geosoft, 2009. GM-SYS Profile Modeling - Gravity and Magnetic Modeling Software for Oasis Montaj (User Guide Ver.4.1).

Ghosh, G.K., 2016. Interpretation of Gravity Data using 3D Euler Deconvolution, Tilt Angle, Horizontal Tilt Angle and Source Edge Approximation of the North-West Himalaya. Acta Geophys. 64 (4), 1112–1138. https://doi.org/10.1515/acgeo-2016-0042.

Goumas, G., 2006. Study of Thriassio Region Structure with Geophysical Methods. M.Sc. thesis. 178p. University of Athens (In Greek).

Grasemann, B., Schneider, D., Stöckli, D., Iglseder, C., 2012. Miocene bivergent crustal extension: evidence from the western Cyclades (Greece). Lithosphere. 4 (1), 23–39.

Hammer, S., 1950. Density determinations by underground gravity measurements. Geophysics 15 (4), 637–652. https://doi.org/10.1190/1.1437625.

Hipkin, R.G., Lagios, E., Lyness, D., Jones, P., 1988. Reference gravity stations on the IGSN71 standard in Britain and Greece. Geophys. J. Int. 92 (1), 143–148. https://doi.org/10.1111/j.1365-246X.1988.tb01128.x.

Hosseini, A.A., Doulati, Ardejani, F., Tabatabaie, S.H., Hezarkhani, A., 2013. Edge detection in gravity field of the Gheshm sedimentary basin. Int. J. Min. Geo-Eng. 47 (1), 41–50. https://doi.org/10.22059/IJMGE.2013.50089.

Iglseder, C., Grasemann, B., Rice, A.H.N., Petrakakis, K., Schneider, D.A., 2011. Miocene south directed low-angle normal fault evolution on Kea Island (West Cycladic Detachment System, Greece). *Tectonics*, 30(4). TC4013, 1–31 https://doi.org/10.1029/2010TC002802.

Karastathis, V.K., Karmis, P., Novikova, T., Roumelioti, Z., Gerolymatou, E., Papanastassiou, D., Liakopoulos, S., Tsombos, G.A., Papadopoulos, G.A., 2010. The contribution of geophysical techniques to site characterisation and liquefaction risk assessment: Case study of Nafplion City, Greece. J. Appl. Geophys. 72 (3), 194–211. https://doi.org/10.1016/j.jappgeo.2010.09.003.

Kessel, G., 1990. Untersuchungen zur Deformation und Metamorphose in Attischen Krystallin, Griechenland. vol. 126. Selbstverlag Fachbereich Geowissenschaften, FU Berlin, pp. 1–150.
Khalil, M.A., Santos, F.M., Farzamian, M., El-Kenawy, A., 2015. 2-D Fourier transform analysis of the gravitational field of Northern Sinai Peninsula. J. Appl. Geophys. 115, 1–10. https://doi.org/10.1016/j.jappgeo.2015.01.022.
Khamies, A.A., El-Tarras, M.M., 2010. Surface and subsurface structures of Kalabsha area, southern Egypt, from remote sensing, aeromagnetic and gravity data. Egyptian J. Remot. Sens. Space Sci. 13 (1), 43–52. https://doi.org/10.1016/j.ejrs.2010.07.006.
Kim, Y.M., Lee, S.M., Okino, K., 2009. Comparison of gravity anomaly between mature and immature intra-oceanic subduction zones in the western Pacific. Tectonophysics 474 (3–4), 657–673. https://doi.org/10.1016/j.tecto.2009.05.004.
Koumetio, F., Njomo, D., Tabod, C.T., Noutchogwe, T.C., Manguelle-Dicoum, E., 2012. Structural interpretation of gravity anomalies from the Kribi–Edea zone, South Cameroon: a case study. J. Geophys. Eng. 9 (6), 664. https://doi.org/10.1088/1742-2132/9/6/664.
Krohe, A., Mposkos, E., Diamantopoulos, A., Kaouras, G., 2010. Formation of basins and mountain ranges in Attica (Greece): the role of Miocene to recent low-angle normal detachment faults. Earth Sci. Rev. 98 (1–2), 81–104. https://doi.org/10.1016/j.earscirev.2009.10.005.
Le Pourhiet, L., Huet, B., May, D.A., Labrousse, L., Jolivet, L., 2012. Kinematic interpretation of the 3D shapes of metamorphic core complexes. Geochem. Geophys. Geosyst. 13 (9), Q09002. https://doi.org/10.1029/2012GC004271.
Leader, L.D., Rawling, T.J., Wilson, C.J.L., 2006. Structural transect and forward modelling of geophysical data across the St Arnaud Group, Victoria. Aust. J. Earth Sci. 53 (5), 863–873. https://doi.org/10.1080/08120090600827504.
Lekkas, E., 2001. The Athens earthquake (7 September 1999): intensity distribution and controlling factors. Eng. Geol. 59 (3–4), 297–311. https://doi.org/10.1016/S0013-7952(00)00119-8.
Lekkas, S., Lozios, S., 2000. Tectonic structure of Mt. Hymittos. Annales Géologiques des Pays Helléniques. vol. 38, pp. 47–62.
Lekkas, E.L., Lozios, S.G., Danamos, G.D., 2001. Geological and tectonic structure of the area between Aigaleo and Parnitha Mt. (Attica, Greece) and their importance to antiseismic planning. Bull. Geol. Soc. Greece 34 (1), 19–27 (*In Greek*). 10.12681/bgsg.16939.
Lekkas, S., Skourtsos, E., Soukis, K., Kranis, H., Lozios, S., Alexopoulos, A., Koutsovitis, P., 2011. Late Miocene detachment faulting and crustal extension in SE Attica (Greece). Geophys. Res. Abstr. 13, EGU2011–13016.
Lepsius, R., 1893. Geologie von Attika. Ein Beitrag zur Lehre von Metamorphismus der Gesteine. Berlin Zeitschr. f. Partkt. Geol. 4 196S, 592p. (In German).
Levy, F., Jaupart, C., 2011. Folding in regions of extension. Geophys. J. Int. 185 (3), 1120–1134. https://doi.org/10.1111/j.1365-246X.2011.05013.x.
Louis, I.F., Karastathis, V.K., Vafidis, A.P., Louis, F.I., 2002a. Resistivity modelling and imaging methods for mapping near-surface features: Application to a site characterization at the ancient Temple of Olympian Zeus in Athens. J. Balkan Geophys. Soc. 5 (4), 135–144.
Louis, I.F., Raftopoulos, D., Goulis, I., Louis, F.I., 2002b. Geophysical Imaging of faults and fault zones in the urban complex of Ano Liosia Neogene basin, Greece: Synthetic simulation approach and field investigations. International Conference on Earth Sciences and Electronics, pp. 269–285.
Lozios, S., 1993. Tectonic analysis of the metamorphic formations of NE Attica. *PhD Thesis*. University of Athens 299p (In Greek). http://hdl.handle.net/10442/hedi/2925.
Makris, J., Yegorova, T., 2006. A 3-D density–velocity model between the Cretan Sea and Libya. Tectonophysics 417 (3–4), 201–220. https://doi.org/10.1016/j.tecto.2005.11.003.
Makris, J., Papoulia, J., Yegorova, T., 2013. A 3-D density model of Greece constrained by gravity and seismic data. Geophys. J. Int. 194 (1), 1–17. https://doi.org/10.1093/gji/ggt059.
Mancinelli, P., Pauselli, C., Minelli, G., Federico, C., 2015. Magnetic and gravimetric modeling of the central Adriatic region. J. Geodyn. 89, 60–70. https://doi.org/10.1016/j.jog.2015.06.008.
Marinos, G., Katsikatsos, G., Georgiadou-Dikeoulia, E., Mirkou, E., 1971. The Athens' schist formation I. Stratigraphy and Structure. Ann. Géol. Pays Hellén. 23, 183–212 (In Greek).
Marinos, G., Katsikatsos, G., Mirkou, E., 1974. The Athens' schist formation II. Stratigraphy and Structure. Ann. Géol. Pays Hellén. 25, 439–444 (In Greek).
Mariolakos, I., Fountoulis, I., 2000. The Athens earthquake September 7, 1999 neotectonic regime and geodynamic phenomena. Ann. Géol. Pays Hellén. 38 (B), 165–174.
Mariolakos, I., Fountoulis, I., Sideris, Ch., Chatoupis, Th., 2001. Morphoneotectonic structure of Parnis Mt. (Attica, Greece). Bull. Geol. Soc. Greece 34 (1), 183–190 (In Greek). 10.12681/bgsg.16965.
Martins-Ferreira, M.A.C., Campos, J.E.G., Von Huelsen, M.G., Neri, B.L., 2018. Paleorift structure constrained by gravity and stratigraphic data: the Statherian Araí rift case. Tectonophysics 738-739, 64–82. https://doi.org/10.1016/j.tecto.2018.05.014.
McPhee, D.K., Langenheim, V.E., Hartzell, S., McLaughlin, R.J., Aagaard, B.T., Jachens, R.C., McCabe, C., 2007. Basin structure beneath the Santa Rosa Plain, northern California: Implications for damage caused by the 1969 Santa Rosa and 1906 San Francisco earthquakes. Bull. Seismol. Soc. Am. 97 (5), 1449–1457. https://doi.org/10.1785/0120060269.
Morelli, C., Gantar, C., Honkasalon, T., McConnel, K., Tanner, J.G., Szabo, B., Uotila, U., Whalen, C.T., 1974. The International Standardization Net 1971 (IGSN71). IUGG-IAG Publ. Spec. 4. Int. Union of Geod. and Geophysics.
Nafe, J.E., Drake, C.L., 1961. *Physical Properties of Marine Sediments*. Technical Report no.2, Lamont Geological Observatory, Palisades, New York. 45p.
Nakada, M., Tahara, M., Shimizu, H., Nagaoka, S., Uehira, K., Suzuki, S., 2002. Late Pleistocene crustal uplift and gravity anomaly in the eastern part of Kyushu, Japan, and its geophysical implications. Tectonophysics 351 (4), 263–283. https://doi.org/10.1016/S0040-1951(02)00161-0.
Nasr, I.H., Amiri, A., Inoubli, M.H., Salem, A.B., Chaqui, A., Tlig, S., 2011. Structural setting of northern Tunisia insights from gravity data analysis Jendouba case study. Pure Appl. Geophys. 168 (10), 1835–1849. https://doi.org/10.1007/s00024-010-0189-7.
Nasuti, A., Pascal, C., Ebbing, J., 2012. Onshore–offshore potential field analysis of the Møre–Trøndelag Fault complex and adjacent structures of Mid Norway. Tectonophysics 518, 17–28. https://doi.org/10.1016/j.tecto.2011.11.003.
Nettleton, L.L., 1939. Determination of density for reduction of gravimeter observations. Geophysics 4 (3), 176–183. https://doi.org/10.1190/1.0403176.
Niedermayer, J., 1971. Die geologische Karte von Athen 1:10.000. Bull. Geol. Soc. Greece 8 (2), 117–134 (*In German*).
Onal, K.M., Buyuksarac, A., Aydemir, A., Ates, A., 2008. Investigation of the deep structure of the Sivas Basin (innereast Anatolia, Turkey) with geophysical methods. Tectonophysics 460 (1), 186–197. https://doi.org/10.1016/j.tecto.2008.08.006.
Papadopoulos, T.D., 2003. Investigation of the deep structure of Central-west Attica with the contribution of geophysical soundings. *OASP Applied research program*, 90p., Athens (*In Greek*) http://www.oasp.gr/assigned_program/2382.
Papadopoulos, T., Alexopoulos, J., Kambouris, P., Tolis, S., Kavounidis, S., 2001. Contribution of modern seismic methods for subsurface investigations. An application at Kalogreza area (Athens). Bull. Geol. Soc. Greece 34 (4), 1317–1323 In Greek. 10.12681/bgsg.17220.
Papadopoulos, T.D., Goulty, N., Voulgaris, N.S., Alexopoulos, J.D., Fountoulis, I., Kambouris, P., Karastathis, V., Peirce, C., Chailas, S., Kassaras, J., Pirli, M., 2007. Tectonic structure of Central-Western Attica (Greece) based on geophysical investigations-preliminary results. Bull. Geol. Soc. Greece 40 (3), 1207–1218. https://doi.org/10.12681/bgsg.16873.
Papaioannou, M., 2002. The Use of Geophysics in the Detection of Underground Structures in Urban Environment. *PhD Thesis*, University of Patras, 125p. (*In Greek*). http://hdl.handle.net/10442/hedi/13562.
Papanikolaou, D., 2015. Geology of Greece. Patakis Publ (440p., Athens (*In Greek*).
Papanikolaou, D., Lozios, S., 1990. Comparative neotectonic structure of high (Korinthia-Beotia) and low rate (Attica-Cyclades) activity. Bull. Geol. Soc. Greece 26, 47–65 (In Greek).
Papanikolaou, D., Lozios, S., Sideris, C., Kranis, H., Danamos, G., Soukis, K., Skourtsos, E., Bassi, E., Marinos, P., Tsiampaos, G., Boukovalas, G., Sabatakakis, N., Antoniou, A., Provia, K., 2002. Geological – Geotechnical study of Athens basin. OASP Applied Research Program 152p., Athens (In Greek). http://www.oasp.gr/assigned_program/2317.
Papanikolaou, D., Bassi, E.K., Kranis, H., Danamos, G., 2004a. Paleogeographic evolution of the Athens basin from upper Miocene to present. Bull. Geol. Soc. Greece 36 (2), 816–825 (In Greek). 10.12681/bgsg.16822.
Papanikolaou, D.I., Lozios, S.G., Soukis, K., Skourtsos, E., 2004b. The geological structure of the allochthonous 'Athens Schists'. Bull. Geol. Soc. Greece 36 (4), 1550–1559 (In Greek). 10.12681/bgsg.16513.
Parasnis, D.S., 1952. A study of rock densities in the English Midlands. Geophys. Suppl. Mon. Not. R. Astron. Soc. 6 (5), 252–271. https://doi.org/10.1111/j.1365-246X.1952.tb03013.x.
Park, C.H., Kim, J.W., Isezaki, N., Roman, D.R., von Frese, R.R., 2006. Crustal analysis of the Ulleung Basin in the East Sea (Japan Sea) from enhanced gravity mapping. Mar. Geophys. Res. 27 (4), 253–266. https://doi.org/10.1007/s11001-006-9006-1.
Sabatakakis, N., 1991. Engineering Geological Setting of Athens Basin. PhD Thesis. University of Patras (216p. In Greek). http://hdl.handle.net/10442/hedi/1734.
Sanchez-Rojas, J., Palma, M., 2014. Crustal density structure in northwestern South America derived from analysis and 3-D modeling of gravity and seismicity data. Tectonophysics 634, 97–115. https://doi.org/10.1016/j.tecto.2014.07.026.
Seman, S., Soukis, K., Stockli, D.F., Skourtsos, E.M., Kranis, H., Lozios, S., 2012. Novel Thermochrono-metric Techniques Applied to the Lavrion Detachment, Lavrion Peninsula, Attica, Greece. Mineral. Mag. 76, 2352 Abstracts.
Seman, S., Soukis, K., Stockli, D.F., Skourtsos, E.M., Kranis, H., Lozios, S., 2013. Provenance of metasediments and Miocene exhumation history of the Lavrion Peninsula, South Attica, Greece: a combined structural, (U-Th)/He, and detrital zircon U-Pb study. Geophys. Res. Abstr. 15, EGU2013–12605.
Smith, N., Cassidy, J., Locke, C.A., Mauk, J.L., Christie, A.B., 2006. The role of regional-scale faults in controlling a trapdoor caldera, Coromandel Peninsula, New Zealand. J. Volcanol. Geotherm. Res. 149 (3–4), 312–328. https://doi.org/10.1016/j.jvolgeores.2005.09.005.
Spector, A., Grant, F.S., 1970. Statistical models for interpreting aeromagnetic data. Geophysics 35 (2), 293–302. https://doi.org/10.1190/1.1440092.
Šumanovac, F., Orešković, J., Grad, M., ALP 2002 Working Group, 2009. Crustal structure at the contact of the Dinarides and Pannonian basin based on 2-D seismic and gravity interpretation of the Alp07 profile in the ALP 2002 experiment. Geophys. J. Int. 179 (1), 615–633. https://doi.org/10.1111/j.1365-246X.2009.04288.x.
Symeonidis, K., Papadopoulos, T.D., Alexopoulos, J., 2005. Use of surface waves for geotechnical characterization of neogene deposits - the Glyfada, Athens case study. Near Surface 2005-11th European Meeting of Environmental and Engineering Geophysics.
Tsokas, G.N., Tsourlos, P.I., Vargemezis, G., Novack, M., 2008. Non-destructive electrical resistivity tomography for indoor investigation: the case of Kapnikarea Church in Athens. Archaeol. Prospect. 15 (1), 47–61. https://doi.org/10.1002/arp.321.
Tsourlos, P.I., Tsokas, G.N., 2011. Non-destructive Electrical Resistivity Tomography Survey at the South Walls of the Acropolis of Athens. Archaeol. Prospect. 18 (3), 173–186. https://doi.org/10.1002/arp.416.
Tzitziras, A., Rozos, D., Vakondios, I., Elias, P., Kynigalaki, M., Nikolaou, N., Konstantopoulou, G., 2000. Macroseismic observations from the earthquake of 7/9/99 in Attiki area. Ann. Géol. Pays Hellén. 38, 145–152 (In Greek).

Weidmann, C., Gimenez, M., Klinger, F.L., Alvarez, O., 2016. Anomalous values of gravity and magnetism in the western margin of Gondwana. Tectonophysics 667, 1–15. https://doi.org/10.1016/j.tecto.2015.11.017.

Whetton, J.T., Myers, J.O., Watson, I.J., 1956. A gravimeter survey in the Craven district of north-West Yorkshire. Proc. Yorks. Geol. Soc. 30 (3), 259–287. https://doi.org/10.1144/pygs.30.3.259.

Wu, H., Li, L., Xing, C., Zhang, S., 2017. A new method of edge detection based on the total horizontal derivative and the modulus of full tensor gravity gradient. J. Appl. Geophys. 139, 239–245. https://doi.org/10.1016/j.jappgeo.2017.02.026.